

ESTIMATION OF THE PETROPHYSICAL PARAMETERS OF SEDIMENTS FROM CHAD BASIN USING WELL LOGS

SANI ALI AND DONATUS M. ORAZULIKE

(Received 22 December 2009; Revision Accepted 7 July 2010)

ABSTRACT

Three petrophysical parameters; shaliness, porosity and thermal conductivity were estimated from well logs obtained from the Faltu-1 well, the Chad Basin. Shaliness was estimated from four independent methods, and trend lines having goodness-of-fit ranging between 0.078 and 0.6801 best describe depth - shaliness variations. The trends were interpreted to predict the lithologies in the formations. Although the shaliness estimates did all agree, the average effective shaliness appears to grow and wane in patterns consistent with geologic history of the basin. Assessment of the contributions of shaliness methods to the effective shaliness revealed dominance of the gamma ray and thorium-based methods over those based on combined bulk density-neutron porosity and self potential. Porosity was estimated from three methods, and polynomial trends having fits ranging between 0.0604 and 0.478 describe depth - porosity variations. Interpretation of the trends revealed lithology trend that agree with the trends of shaliness. Estimates of average effective porosities of formations favorably compared with measurements, while analysis of the plots of various functions of porosity with depth allowed for the estimation of the porosities at deposition. Three independent methods were employed to estimate thermal conductivities. Trends having fits ranging between 0.1202 and 0.7996 best describe the variations of the parameter with depth. The trends also revealed similar lithology structure as did trends of shaliness, and appear to wane and grow in patterns opposed to those of the shaliness. Variations of the well site average thermal conductivities appear to trend with the structural highs. Assessment of the methods ranked their contributions to the effective thermal conductivity.

KEY-WORDS: effective shaliness, effective porosity, porosity at deposition, effective thermal conductivity, Chad Basin

INTRODUCTION

Six sedimentary formations have been delineated in the Nigeria sector of the Chad Basin (Carter et al., 1963). These are the Bima Sandstones, the Gongila, the Fika, the Gombe Formations, the Kerri Kerri and Chad Formations. The purpose of this article is to estimate three related petrophysical parameters, namely, thermal conductivity, porosity and shaliness (clay volume) of these sedimentary formations as encountered in an exploratory well, the Faltu-1, drilled in the Chad Basin, N.E. Nigeria using log data.

Thermal conductivity is an intrinsic property that exercises first-order control on temperature distribution as well as on heat flow pattern within basins (Onuoha and Ekine, 1999). The thermal conductivity of a rock depends on the conductivities and geometrical arrangement of its constituent minerals and fluid content (Kappelmeyer and Hanel, 1974; Beck, 1976; Vassuer et al., 1995), as well as on the ambient temperature and pressure (Sekiguchi, 1984; Clauser and Huenges, 1995). The thermal conductivity estimates along with temperature gradient allow for the computation of the heat flow, and hence the assessment of the evolution of the basin and maturation. The thermal regime operating within a sedimentary basin is needed for the understanding of the origin of the basin as well as for formation of certain mineral resources occurring therein. The porosity of the sediments allows for reserves estimation, while shaliness allows for assessment of

reservoir rocks quality. Indirectly also, porosity influences the modelling of heat flow, subsidence history, and the maturation and migration of hydrocarbons and other geofluids.

GEOLOGIC SETTING

The Chad Basin is the largest inland basin in Africa. It is one of several basins within the West and Central African Rift System, and is genetically related to the Benue Trough, with the two making up the third and failed arm of a triple junction rift system that preceded the opening of the South Atlantic and the subsequent separation of African and South American continents (Burke, 1976). It consists of several sub-basins spread around the republics of Niger, Chad, Cameroon and Nigeria. Cratchley (1960) has further delineated the Nigerian sector into three sub-basins for hydrocarbons exploration, and are separated from each other (Fig. 1) by the Arege - Marte High, the Bama Ridge, the Maiduguri and the Gubio Highs (GeoEngineering International, 1994; Obi, 1996).

The generalized stratigraphic framework consists of six units (Fig. 2). The basal units are the Bima Sandstones. These sequences of sandstones, mudstones and occasional shales (Carter et al., 1963) were deposited in the Aptian - Albian (Genik, 1992), and unconformably overlies the Basement Complex. The wide variation in lithology, texture, colour and structure have suggested to its division into three separate

Sani Ali, Physics Programme, A.T.B. University, Bauchi, Nigeria.

Donatus M. Orazulike, Geology Programme, A.T.B. University, Bauchi, Nigeria.

formations, the Lower, Middle and Upper Bima Formations. The thicknesses encountered in drilled holes range up to 1.5 km while interpreted seismic sections (Avbovbo et al., 1986) suggests 4.5 to 5.5 km depth extent. Mudstone and shale horizons in the Upper Bima have yielded Total Organic Content, TOC, of between 0.09 and 0.82 wt per cent (GeoEngineering International, 1994), while sandstone horizons have porosities in the range of 5.58 % to 29.22 % but which averaged 13.74 % (Samaila, 2007). Overlying the Bima Formation is the transitional Gongila Formation, deposited from the Late Albian to the Early (Reyment, 1980; Allix *et al.*, 1981; Benkheilil and Robineau, 1983; Genik, 1992). The formation consists of fine- to very fine-grained sandstone beds and shale beds, becoming sandier towards the base. The Fika Formation, consisting of a sequence of marine blue-black shales containing one or two thin non-persistent limestone horizons, conformably overlies the Gongila Formation. This was deposited at the height of the marine transgression of the area between Late Cenomanian and end of Turonian, and may be up to 1000 m thick. Although lacking in reservoir-type rocks, horizons rich in

source-type rocks have yielded TOC in the range 0.37 to 1.40 wt per cent (Robertson Group, 1989, 1991). The Gombe Formation, a sequence of sandstone, shale, ironstone and coal beds that may be up 1000 m thick, was deposited in estuarine to deltaic environment over the Fika Formation. The occurrence of the formation is restricted to the western part of the basin. The Kerri Kerri Formation overlies by the Gombe Formation at an angular unconformity. It consists of flat-lying grits, sandstones and clays, and deposited in the Late Maastrichtian to Paleocene. The Chad Formation, a sequence consisting of mostly massive and gritty clays, loosely to uncemented sands and silts overlies the Kerri Kerri Formation over a minor unconformity (Avbovbo et al., 1986). It was deposited during the Middle Neogene to Quaternary up to Recent (Carter et al., 1963). These are composed of fine- to coarse-grained, highly- to loosely-cemented sands separated by thick clay and sandy clay beds. Doleritic intrusives and gabbros, similar to the sills and dykes encountered in wells in the Lake Chad, Chad Republic (Genik, 1993), are common (Robertson Group, 1989, 1991; GeoEngineering International, 1994).

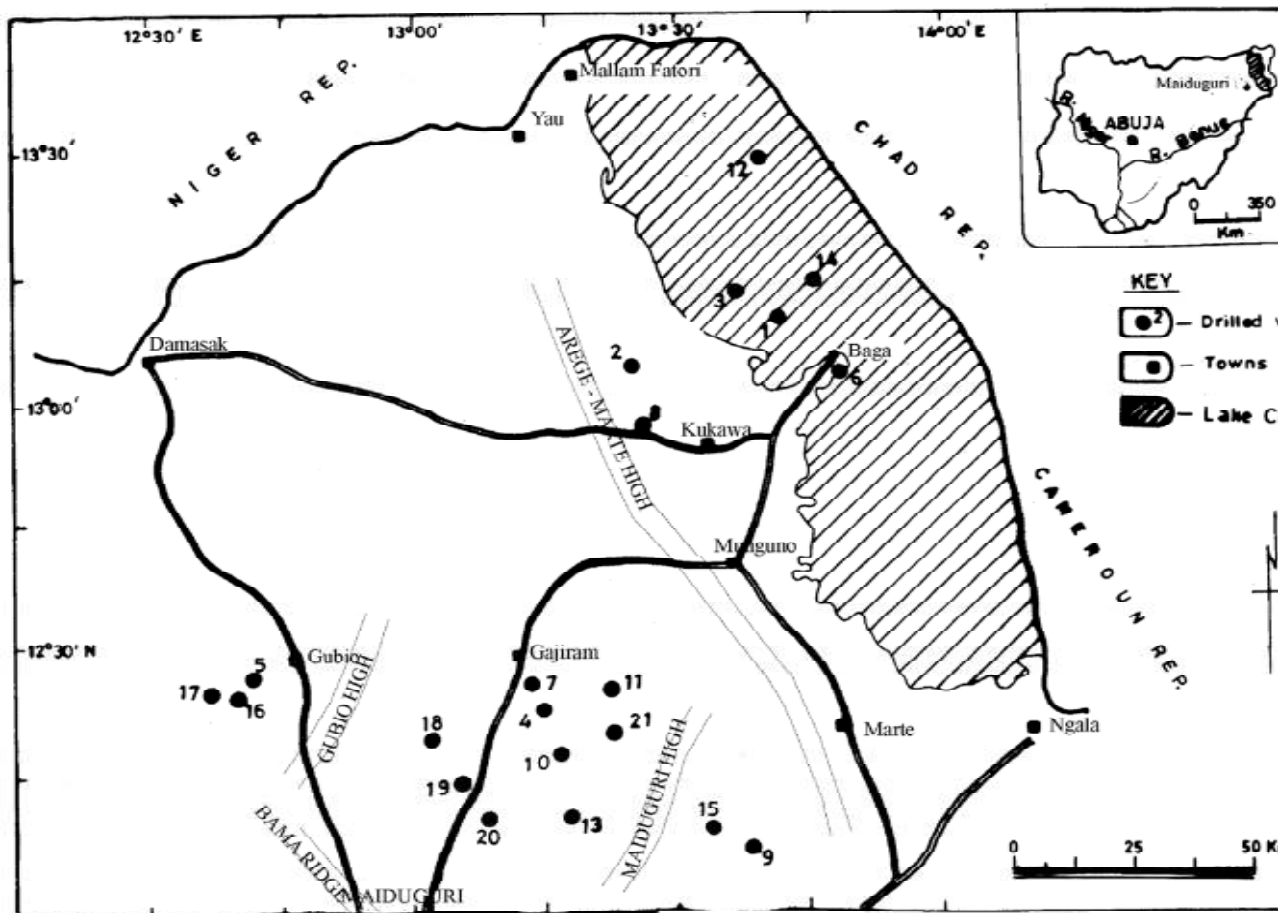


Fig 1. Location map of the study area. The wells marked 1, 2, 3, ... 21 are respectively the Albarka-1, the Bulte-1, the Faltu-1, the Gaibu-1, the Gubio SW-1, the Herwa-1, the Kanadi-1, the Kasade-1, the Kamar-1, the Kinsar-1, the Krumta-1, the Kuchalli-1, the Masu-1, the Mbeji-1, the Murshe-1, the Ngamma East-1, the Ngor North-1, the Sa'a-1, Tuma-1, Wadi-1 and the Ziye-1 wells.

System	Geochronology		Volcanism	Deposition Environment	Formation	Thickness (m)	Description
	Series/ Stage	Age (Ma)					
Quaternary	Holocene/ Pleistocene	0	vv	Continental	Chad	200 - 600	Clays with sands interbeds
		5.2					
Tertiary	Miocene/ Pliocene	66.5		Continental	Kerri Kerri	250 - 1100	-Iron-rich sandstones, clays and laterite
Cretaceous	Maastrichtian	74		Estuarine deltaic	to Gombe	0 - 1000	Sandstones, siltstones, shales and clays with limestone beds
	Campanian	84		Marine	Fika	300 - 1200	-Shale, dark gray to black, gypsiferous with limestone and sandstone beds
	Santonian	88					
	Coniacian	92					
	Senonian	96					
	Turonian	108		Transitional	Gongila	200 - 1500	-Alternating sandstones and shales with limestone beds
	Albian	113	Continental	Bima (Upper)	2000 - 8600	-Sandstones, gravelly to medium grained, poorly sorted and highly feldspatic	
	Aptian			Bima (Middle)			
			Bima (Lower)				
Pan-African Precambrian Basement							

Fig. 2: Generalised stratigraphic column for the Nigerian sector of the Chad basin

DATA ACQUISITION

The well log data used in this study were recorded as part of the Chad Basin Petroleum Exploration - Drilling Programme of the Nigerian National Petroleum Corporation, NNPC. Ten log types were required for the estimation of the petrophysical parameters of interest: shaliness, porosity and thermal conductivity. These are the gamma ray (*GR*), compressional and transverse sonic, spontaneous potential (*SP*), bulk density (*RB*), neutron porosity (*NP*), thorium (*TH*), potassium (*PO*), and uranium (*UR*) spectral gamma ray and photoelectric capture cross section factor (*PEF*) logs. In addition to these, the caliper (*CAL*) log is also required to determine the structural states of a drilled hole as the readings of some of the recording tools in the hole are affected by its structural state. The required data were obtained from the Falu-1 well. This well was drilled to a total depth of 3160 m. Data from *CAL*, compressional sonic, *GR* and *SP* logs are available from the depth of 50 m to total depth, those from *RB*, *NP* and *PEF* logs from the depth of 550 m to total depth, while those from the *PO*, *UR*

and *TH* logs from the depth of 1360 m to total depth. Transverse sonic log data are completely unavailable. The scale of the logs allowed the picking of the curves at intervals no smaller than 2 m. These picking points constitute the horizons at which the petrophysical parameters were calculated. Data on the thicknesses of formations was obtained from the report of GeoEngineering International (1994) which is a review of previous studies by the Robertson Group in 1989 and 1991 carried out for the NNPC.

COMPUTATIONS OF SHALINESS

The shaliness of drilled sedimentary rocks was estimated using four independent methods. The first method used the *GR* log. After correction for the effect of uranium, the log readings the log readings against thick shale (maximum) and thick sand (minimum) formations were noted. The shaliness at each drilled depth, V_{GR} , was calculated using the equations of Serra et al., (1980) and Dresser Atlas (1982) depending on degree of consolidation of the drilled lithology. A drilled lithology is considered consolidated when its *CAL* log

reading does not exceed the size of the bit used in drilling it by more than 25 %. Where the size of the drilled hole is more, the lithology is considered unconsolidated, and the appropriate equations were employed to compute the shaliness. The second set of the estimates of shaliness, V_{SP} , were calculated from the *SP* log using the equation of Asquith and Gibson (1991), Rider (1991) and Beardsmore and Cull (2001), the third set, V_{TH} , were calculated from the *TH* log using equations of Rider (1991). The shaliness of shallower formations could not be obtained due to the absence of the *TH* log from the depths of 50 to 1360 m. The last set of the estimates of shaliness, V_{d-n} , were estimated from a combination of *NP* and *RB* logs using equations of Beardsmore and Cull (2001). Availability of *RB* and *NP* logs from the depth of 550 m meant that shaliness of shallower formations could not be estimated by the method.

Shaliness estimates greater than 1.0, the maximum for pure shale lithology, as well as those less than zero, the minimum for pure quartz lithology were assumed to be in error, and excluded from further use. The availability of more than one independent shaliness estimate at each drilled depth allowed for the use of the method of Asquith (1991), Hunt and Pursell (1997) and Beardsmore and Cull (2001) to estimate the effective shaliness, V_{eff} , as the minimum of the estimates. Table 1 gives the estimates of the average shaliness at the levels of the drilled column and formations by all the methods.

Figs. 3 to 7 are plots of depth versus shaliness estimates for the Chad, the Kerri Kerri, the Fika, the Gongila and the Bima Formations respectively, and Fig. 8 is a similar plot for the whole drilled column. The blue, pink, yellow, plum and red coloured curves in the figures respectively represent the best fitting polynomial trends describing the variations of V_{GR} , V_{SP} , V_{d-n} , V_{TH} and V_{eff} with depth, while the coloured-matched text boxes give the corresponding polynomial equations and goodness-of-fits. For the Chad Formation (Fig. 3), V_{GR} estimates are best described by fifth degree polynomial trend with moderate goodness-of-fit of 0.596, while those of V_{SP} are best described by a power function of the depth with a better but still moderate fit of 0.680. The figure also shows that V_{eff} is also best described by a fifth degree polynomial trend. The trend of V_{GR} is interpreted indicate three lithologies, with the top lithology having shaliness that increases with depth and which is interpreted to suggest a facie that is coarsening upward, and therefore regressive deposition environment. The bottom lithology has shaliness decreasing with dept, and is interpreted to indicate an upward fining facies and therefore suggesting a transgressive deposition environment. The middle lithology, which extends for about 190 m, has a depth-invariant shaliness of about 0.320. While failing to indicate the three lithologies, the trend of V_{SP} indicates rather a steady depth-increasing shaliness, and is interpreted to suggest impermeability in the formation. The trend of V_{eff} although best described by a fifth degree polynomial as the trend of V_{GR} , closely agrees with the trend of V_{SP} up the depth of about 330 m, and with V_{GR} for the rest of the depth extent of the formation. The close correlation between V_{eff} and V_{SP} is interpreted to indicate that the *SP* log is a better shaliness indicator for the top two lithologies of

the formation while the *GR* log is better for the deeper lithology. The trend is also interpreted to indicate two lithologies in contrast to three suggested by V_{GR} .

Fig. 4 gives the depth versus shaliness estimates plots for the Kerri Kerri Formation. Values of V_{d-n} are higher than those of all other methods, and their trend is described by a sixth degree polynomial with a moderate fit of 0.5007. Although not contributing to V_{eff} at any point along the whole length of the formation, the trend of V_{RB-NP} is interpreted to indicate a three-lithology formation. The trend of V_{SP} is also best described by a sixth degree polynomial with a moderate fit of 0.5031 in which shaliness generally increases with depth, and contributes to V_{eff} only for the top 20 m of the formation. The trend is interpreted to blurredly indicate a three-lithology formation as outlined by the trend of V_{RB-NP} , as well as to indicate permeability in lithologies. The trend of V_{GR} , best described by a fifth degree polynomial having a moderate fit of 0.565, shows shaliness decreasing with depth for depth range of 490 to 1160 m, but which reverses thereon for the rest of the depth extent of the formation. Except for the top 20 m, V_{GR} contributes to V_{eff} for all the depth extent of the formation. While the trend is interpreted to indicate upward fining facies and therefore suggesting a transgressive deposition environment, it could only be interpreted to indicate a two-lithology formation, failing to indicate the top lithology. The trend of V_{eff} is described by a sixth degree polynomial having a moderate fit of 0.576. The trend closely follows that of V_{GR} for the entire length of the formation except the top 120 or so metres, and is interpreted to indicate three lithologies in contrast to two indicated by V_{GR} . The closeness of the two trends is interpreted to suggest that V_{GR} is the better shaliness indicator in the formation in comparison to V_{SP} and V_{d-n} .

Fig. 5 gives the plots for the Fika Formation. Except at the two depth intervals of 1840 to 1900 and 1960 to 2060 m, estimates V_{d-n} are at all points higher than those of all other methods, giving a trend that is best described by a sixth degree polynomial having a moderate fit of 0.581. The trend of V_{SP} is also described by sixth degree polynomial having a low fit of 0.2709. While not approaching V_{eff} at any pint along the depth extent of the formation, both trends are interpreted to indicate two lithologies, the top lithology extending up to about 1520 m and the second from thereon, with the two depth intervals mentioned above seen as intrusions. The trend of V_{TH} is also described by sixth degree polynomial having a low fit of 0.1685, and approaches V_{eff} only at the top of the formation. Although the trend could not be interpreted to indicate the two lithologies indicated by trends of both V_{d-n} and V_{SP} , it however clearly indicates the two intrusive bodies. The trend of V_{GR} is also described by a sixth degree polynomial having a low fit of 0.3049. Except for a short depth interval not more than 40 m towards its top, it approaches V_{eff} for the entire depth extent of the formation. While the trend could only be blurredly interpreted to suggest a two-lithology formation, it however clearly indicates the two possible intrusive bodies. The pattern of the trend is interpreted to indicate upward fining facies, and therefore a transgressive deposition environment. Like other trends, V_{eff} trend is also best described by sixth degree polynomial having a low fit of 0.3049. Its

closeness in trend and value to the V_{GR} allowed it to be similarly interpreted.

The depth versus shaliness plots for the Gongila Formation is given in Fig 6. In comparison to other shaliness trends, the trends for this formation, described by low-fitting sixth degree polynomials, are least scattered, indicating closer agreement. The trend for V_{d-n} , while not approaching V_{eff} at any point along its entire depth extent, is interpreted to indicate a two-lithology formation, with the possibility of two smaller others at its top and base. Trend of V_{SP} approaches V_{eff} only between the depths of 2250 and 2370 m. It appears invariant except at its top, and could therefore not be interpreted to indicate the possible lithologies, but rather to indicate its impermeability. The trend of V_{GR} approaches V_{eff} only for the top 30 m, and is also interpreted to indicate a two lithologic-formation with the possibility of two others at its top and base. The pattern of the trend did not give insight into the environment of deposition, but between the depths of 2500 and 2750 m, all three trends of V_{GR} , V_{SP} and V_{d-n} appear to be in agreement. Except for the top 150 m, the trend of V_{TH} approaches V_{eff} for the depth extent of the formation and is interpreted to indicate a two-lithology formation but with the possibility of only a third at its base. Similarity in the shapes of the trends of V_{eff} and V_{GR} allowed the interpretation V_{eff} in a like manner. Fig. 7 gives the depth versus shaliness plots for the Bima Formation. All five shaliness trends are described by sixth degree polynomials having low to moderate fits, with the trend of V_{TH} approaching that of V_{eff} for the entire depth extent of the formation. The trends for V_{SP} , V_{TH} , V_{d-n} and V_{eff} give similar patterns that are interpreted to indicate a five-lithology formation, while the trend of V_{GR} could not be so interpreted. The trend of V_{SP} is further interpreted to indicate permeability in the lithologies.

Fig. 8 gives the depth versus shaliness plots of the trends of all five shaliness estimates along the drilled column. The plots appear to confirm the patterns of shaliness observed in the formations, with sixth degree polynomials having low, less than 0.300, to moderate, less than 0.700, fits best describing their trends. The trends are broadly interpreted to indicate shaliness raise and wane with the marine transgression and regression of the area. The trend of V_{SP} , best described by

quadratic function with a slightly-improved but still moderate fit of 0.6553 is interpreted to indicate similar phenomenon but with less sensitivity to indicate fluctuations highlighted by other methods.

Table 1 indicates that the Fika Formation, a shale sequence is the shaliest, with an average effective shaliness of 0.145 ± 0.003 . The Chad and the Gongila Formations are the next shaliest, with average effective shaliness of 0.138 ± 0.001 and 0.135 ± 0.001 respectively, while the Kerri Kerri and Bima Formations are the cleanest, having average effective shaliness of 0.100 ± 0.001 and 0.061 ± 0.009 . The shaliness estimates are consistent TOC (Robertson Group, 1989 and 1991; GeoEngineering International, 1994). The pattern of average effective shaliness appears to follow the growth and wane of the marine invasion of the area, similar to the pattern indicated by the depth versus shaliness plots. Patterns of average V_{TH} , V_{d-n} and V_{SP} appear to agree with the above pattern for V_{eff} , while V_{GR} slightly differs.

The four shaliness methods have equal chances of contributing to V_{eff} , which is obtained as the least of the estimates by the methods. If a single method were to contribute to V_{eff} , a cross plot of V_{eff} against shaliness estimate for the method would be a straight line, at an angle of 45° from both axes and having a goodness-of-fit of unity for the linear line. If however V_{eff} were to be contributed by more than one method, the cross plot of V_{eff} against each of the shaliness estimates by the methods would have a fit less than unity. Figs. 9a to f are cross plots of V_{eff} versus V_{GR} , V_{SP} , V_{d-n} and V_{TH} for the five formations as well as for the drilled column. The regression equations expressing the relation between the two estimates of shaliness as well as the goodness-of-fits are listed on the figures. With goodness-of-fits of 0.4375, 0.9232 and 0.8666 respectively for the Chad, the Kerri Kerri and the Fika Formations, V_{GR} appears to be a better contributor to V_{eff} in comparison to the other shaliness estimates. Similarly also, V_{TH} is a better contributor to V_{eff} with goodness-of-fits of 0.7417 and 0.7265 for the Gongila and Bima Formations. The goodness-of-fit of 0.5699 and 0.5765 respectively for V_{GR} and V_{TH} for the whole drilled column suggests that the contributions of the two shaliness methods to V_{eff} are nearly equal.

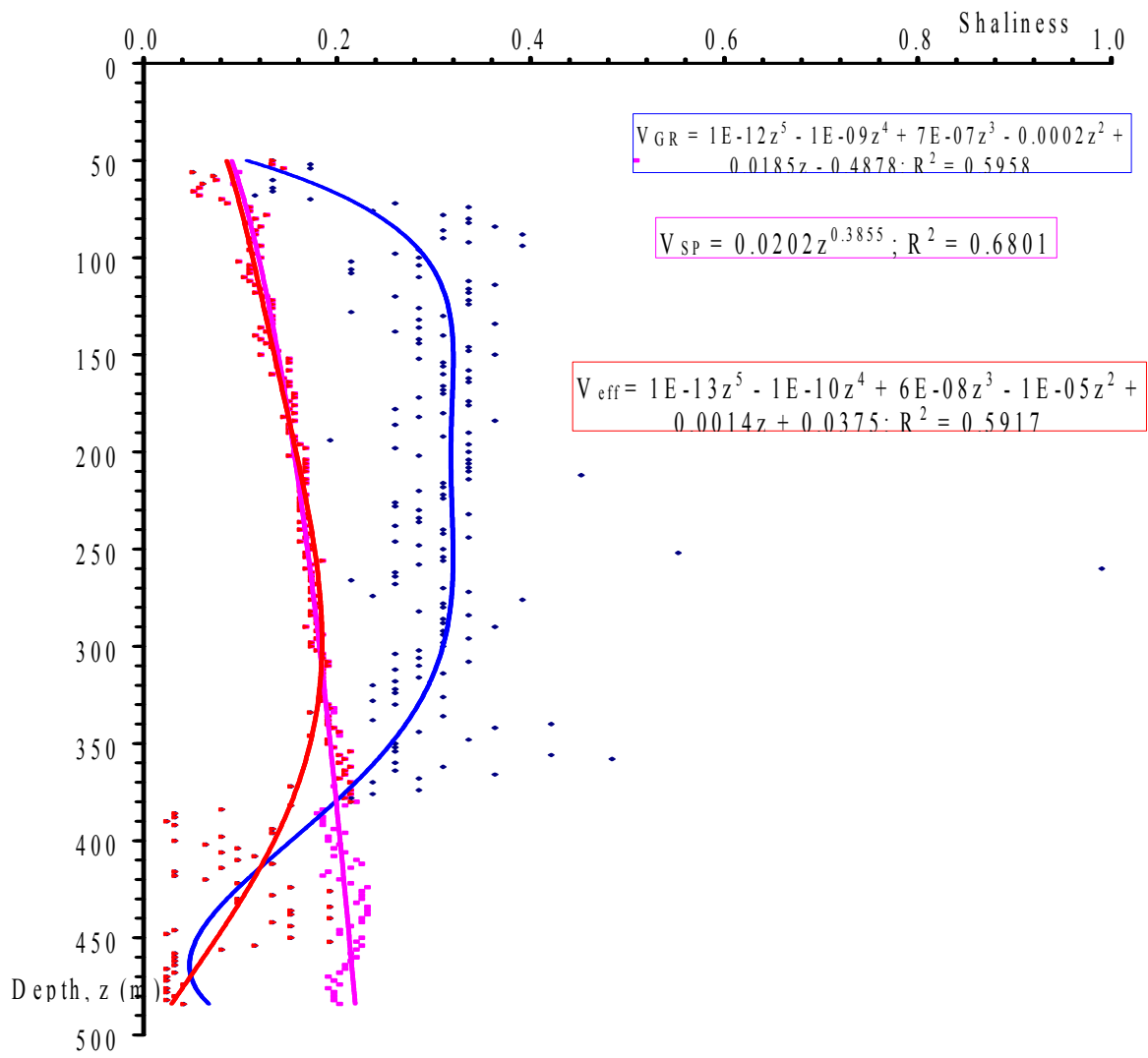


Fig. 3. Depth versus shaliness plots for the Chad Formation. Blue, pink and red curves are for V_{GR} , V_{SP} and V_{eff} respectively.

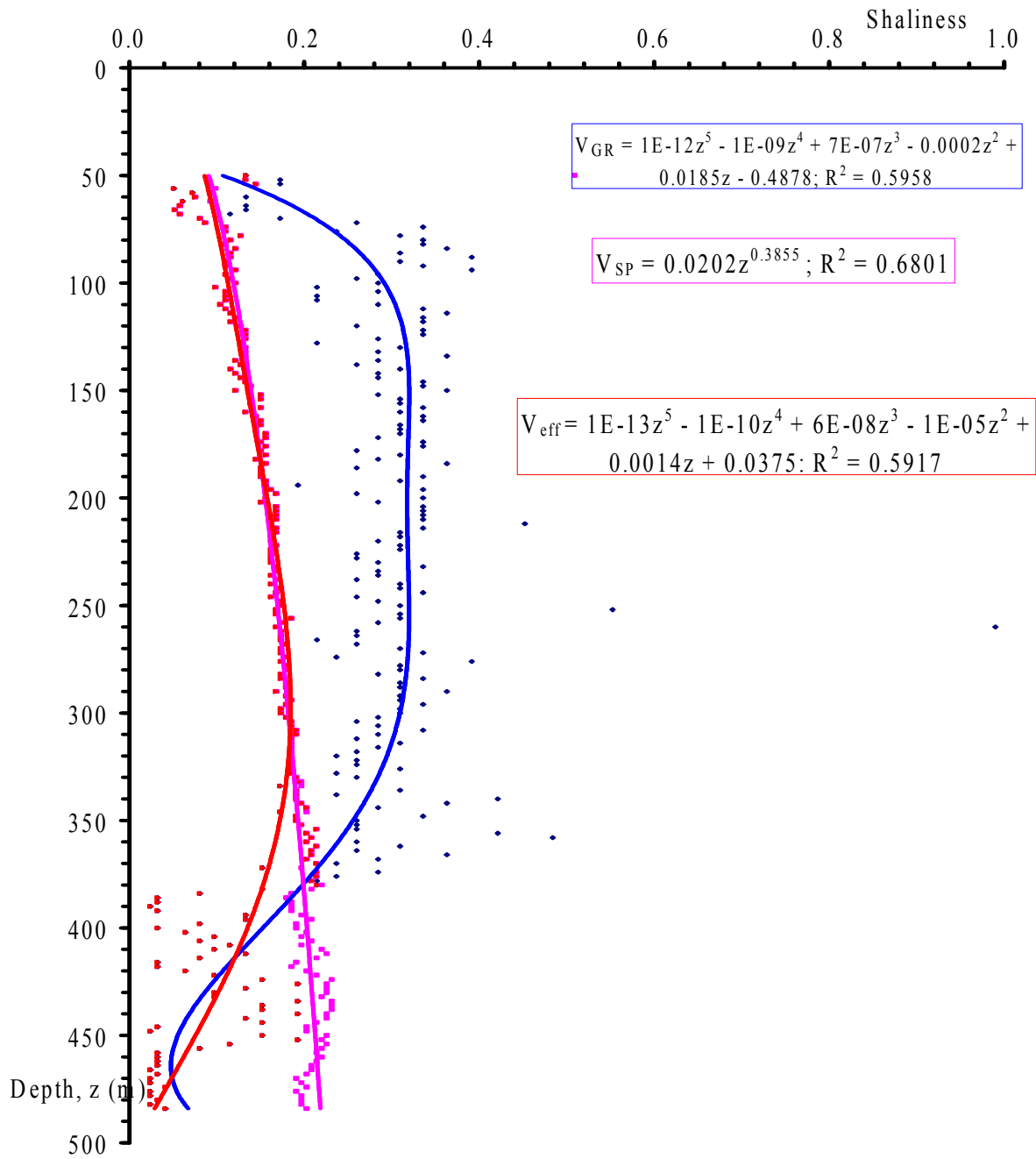


Fig. 4. Depth versus shaliness plots for the Kerri Kerri Formation. Blue, pink, yellow and red curves are for V_{GR} , V_{SP} , V_{d-n} and V_{eff} respectively.

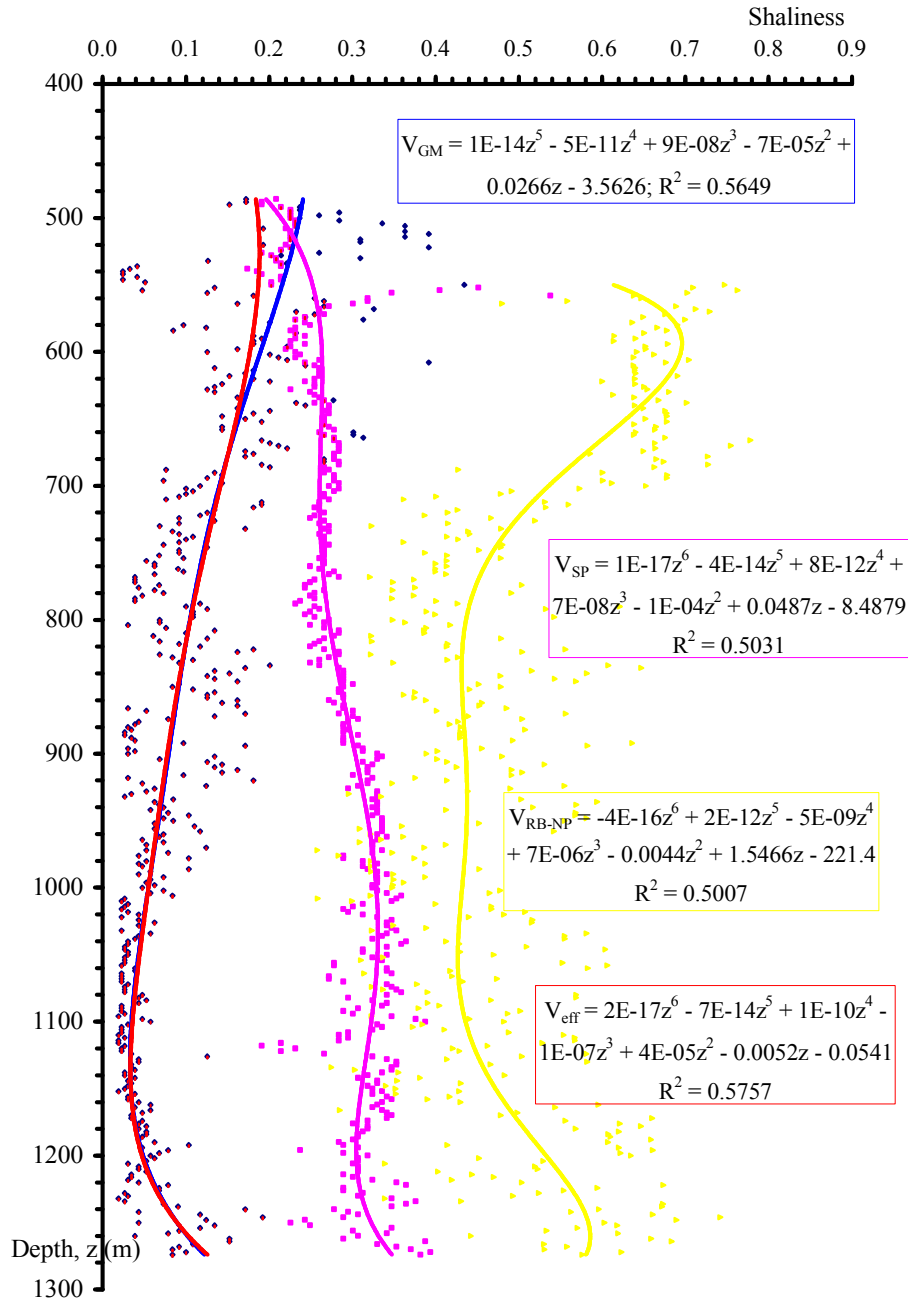


Fig. 5. Depth versus shaliness plots for the Fika Formation. Blue, pink, yellow, plum and red curves are for V_{GR} , V_{SP} , V_{d-n} , V_{TH} and V_{eff} respectively.

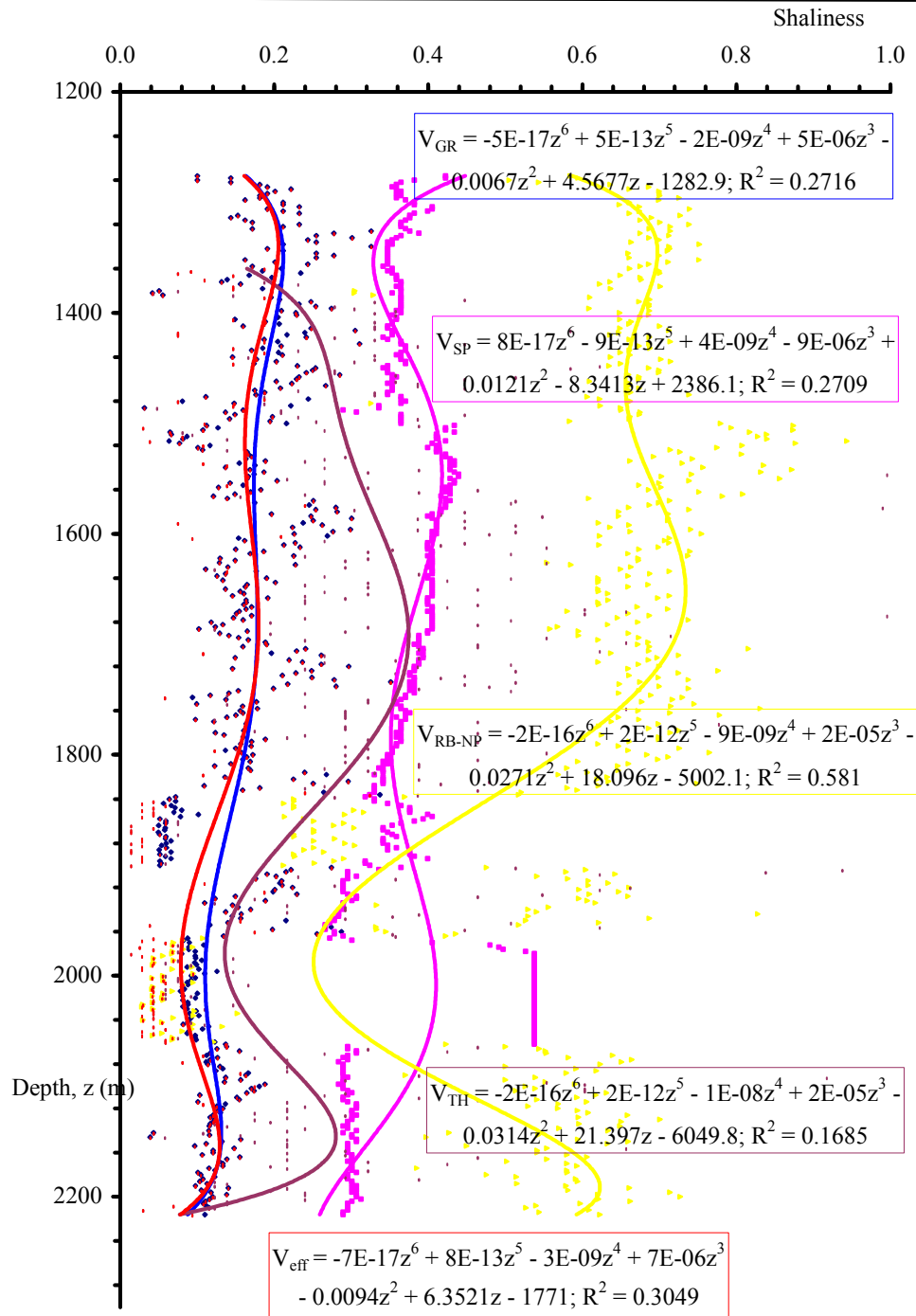


Fig. 6. Depth versus shaliness plots for the Gongila Formation. Blue, pink, yellow, plum and red curves are for V_{GR} , V_{SP} , V_{d-n} , V_{TH} and V_{eff} respectively.

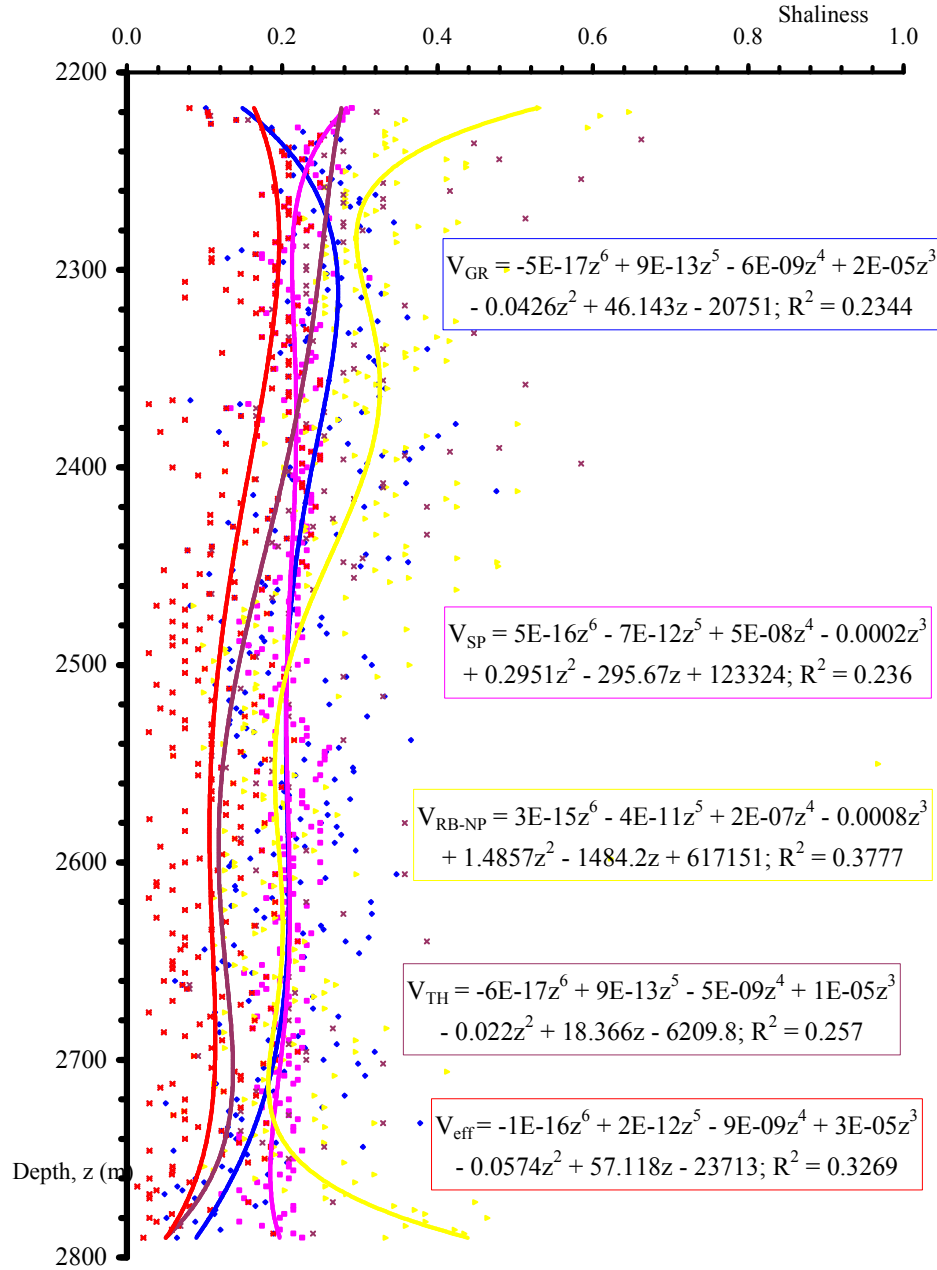


Fig. 7. Depth versus shaliness plots for the Bima Formation. Blue, pink, yellow, plum and red curves are for V_{GR} , V_{SP} , V_{d-n} , V_{TH} and V_{eff} respectively.

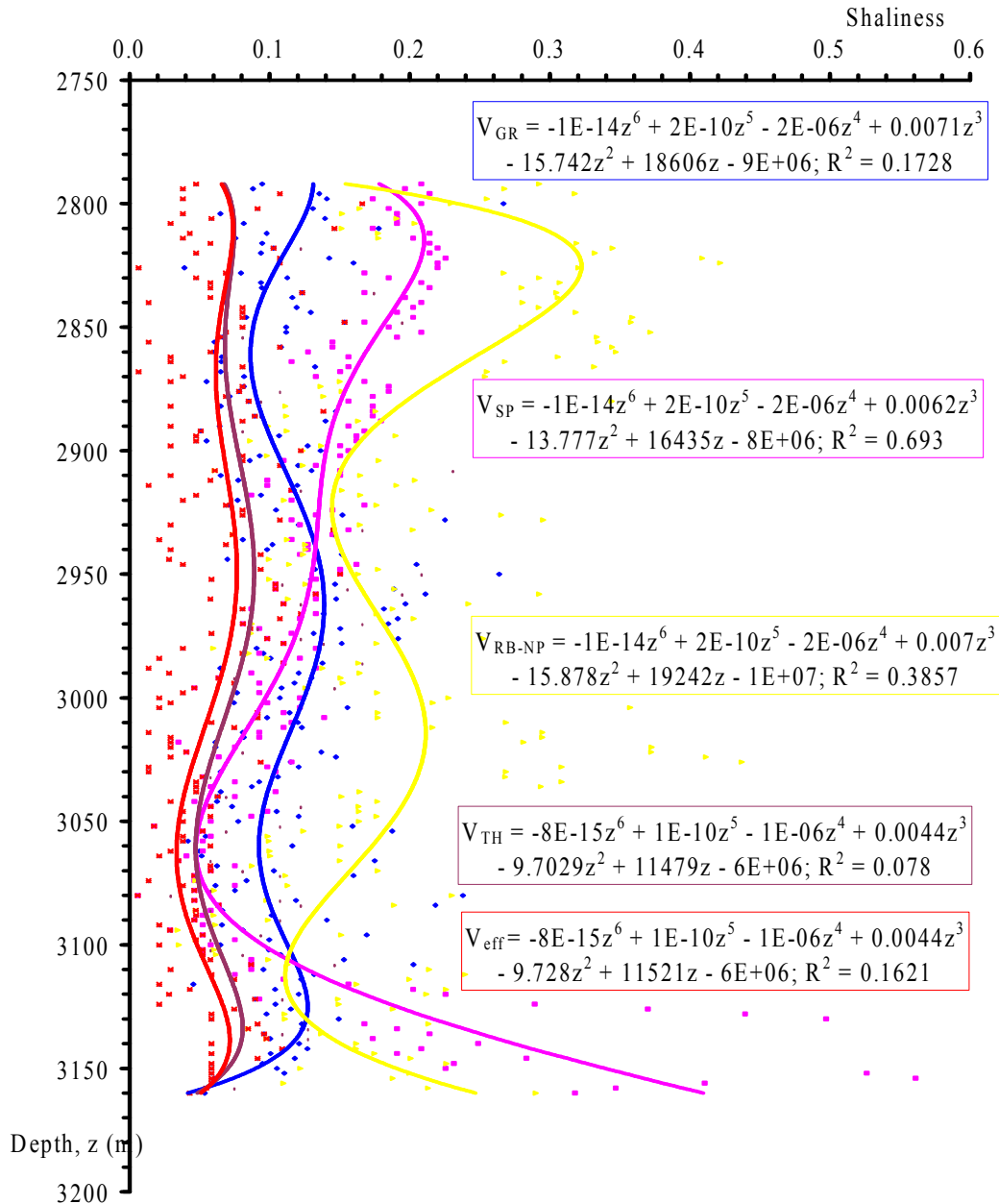
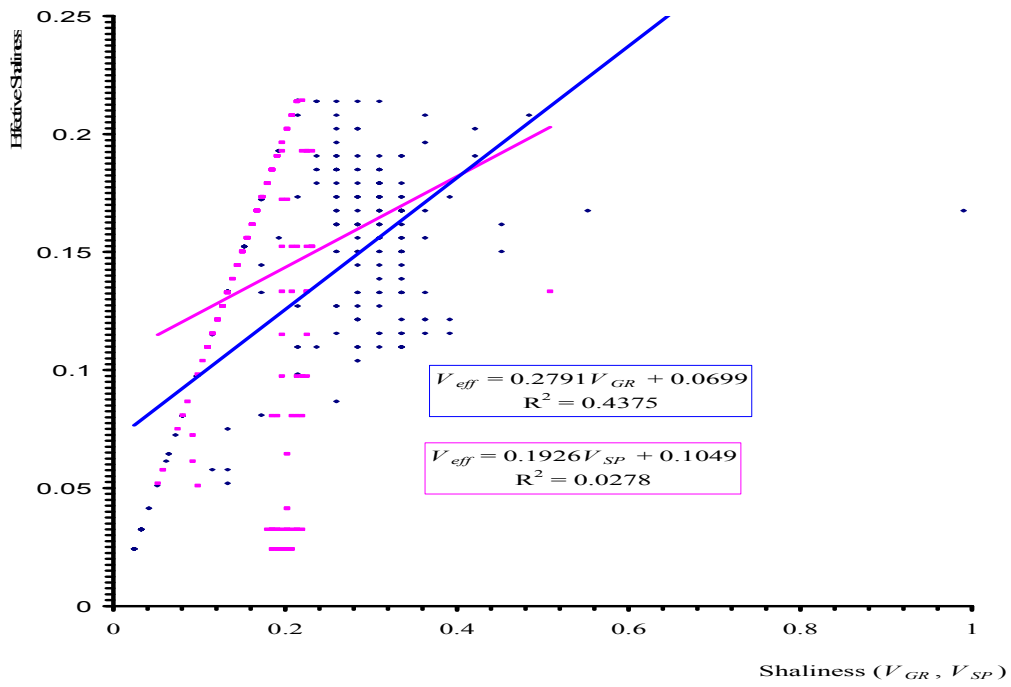


Fig. 8. Depth versus shaliness plots for the drilled column in the Falu-1 well. Blue, pink, yellow, plum and red curves are for V_{GR} , V_{SP} , V_{d-n} , V_{TH} and V_{eff} respectively.

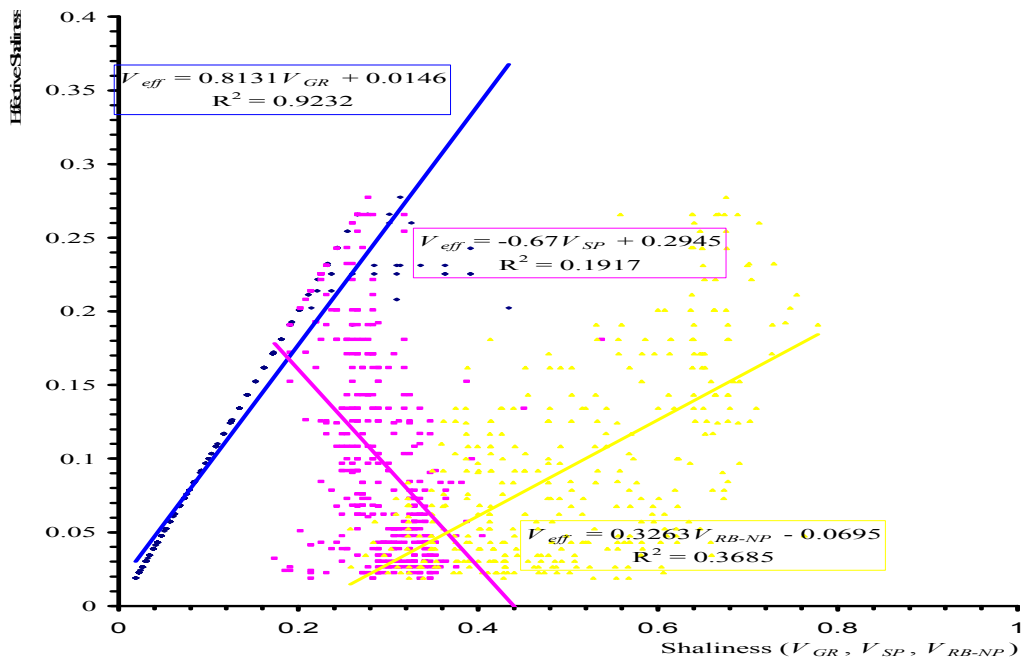
Table 1. Average shaliness of formations in the Falu-1 well. V_{GR} , V_{TH} , V_{d-n} and V_{SP} are average shaliness estimated from the GR, thorium, combined bulk density and neutron porosity, self potential logs, while V_{eff} is the average effective shaliness.

Formation	V_{GR}	V_{SP}	V_{d-n}	V_{TH}	V_{eff}
Chad	0.243 ± 0.008	0.170 ± 0.003	-	-	0.138 ± 0.004
Kerri Kerri	0.106 ± 0.004	0.290 ± 0.002	0.502 ± 0.006	-	0.100 ± 0.004
Gombe	-	-	-	-	-
Fika	0.157 ± 0.003	0.373 ± 0.003	0.562 ± 0.010	0.261 ± 0.009	0.145 ± 0.003
Gongila	0.211 ± 0.005	0.210 ± 0.002	0.257 ± 0.007	0.170 ± 0.007	0.135 ± 0.004
Bima	0.111 ± 0.003	0.143 ± 0.006	0.192 ± 0.007	0.071 ± 0.003	0.061 ± 0.002
Column	0.161 ± 0.002	0.266 ± 0.003	0.426 ± 0.006	0.193 ± 0.005	0.121 ± 0.002

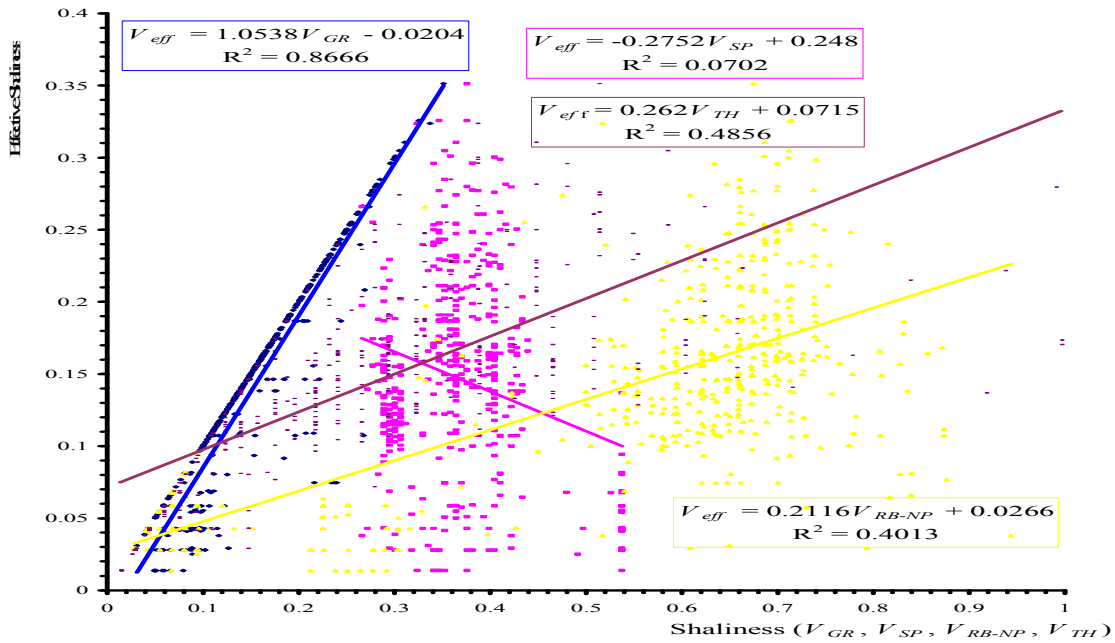
(a)



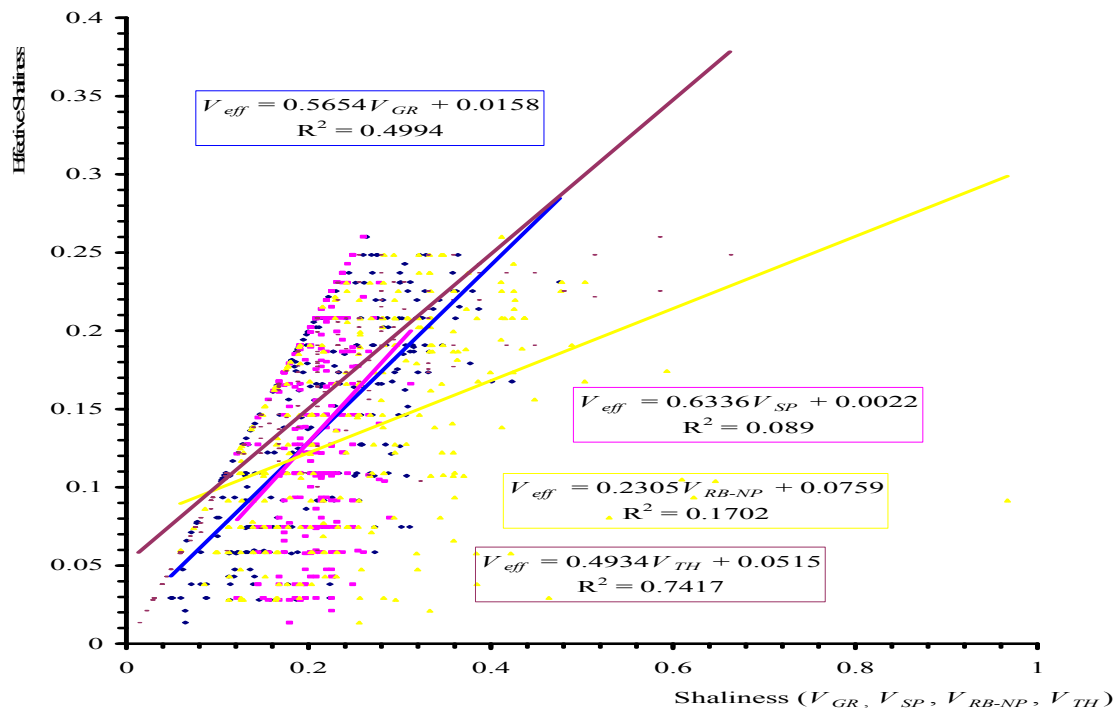
(b)



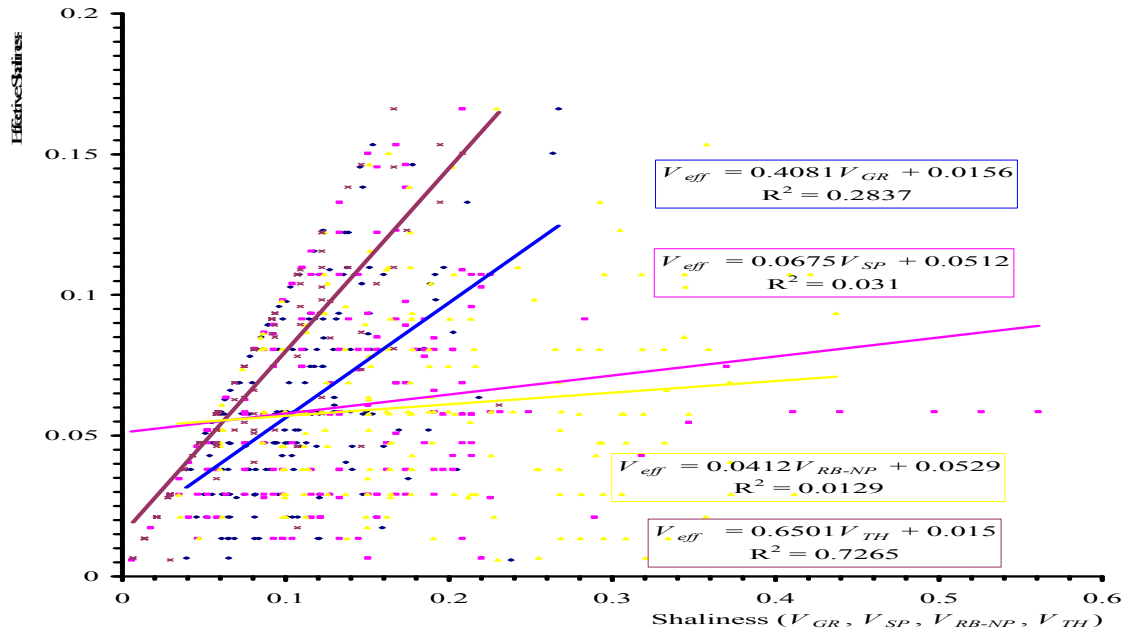
(c)



(d)



(e)



(f)

Fig. 9. Cross plots of the effective shaliness versus shaliness estimates by the four methods for the five formations encountered in the Faltu-1 well. (a) Chad Formation, (b) Kerri Kerri Formation, (c) Fika Formation, (d) Gongila Formation, (e) Bima Formation, and (f) the drilled well. The blue, pink, yellow, plum and red lines are for V_{GR} , V_{SP} , V_{d-n} , V_{TH} and V_{eff} respectively.

POROSITY COMPUTATIONS

Three porosity estimates of the drilled sedimentary rocks in the Faltu-1 well, φ_{son} , φ_{den} and φ_{d-n} , were calculated using separate methods. The first method, (Schlumberger, 1972), employs data from the *RB* log while the second (Wyllie et al., 1958 and Beardsmore and Cull, 2001) uses data from the sonic or interval transit time (Δt) log. The last method (Asquith and Gibson, 1982 and Rider, 1991) employs a combination of *RB* and *NP* logs. Porosity estimates greater than or equal unity, the maximum possible, and those less than zero, the minimum possible, were assumed to be in error, and excluded from further use. The first two methods also requires the interval transit times (Δt_{ma} and Δt_f) as well as densities (ρ_{ma} and ρ_f) of matrix materials and the pore fluids. Δt_{ma} and ρ_{ma} were assigned values of $181.88 \mu s m^{-1}$ and $2650 kg m^{-3}$ respectively, while the pore fluid, assumed to be water, was assigned Δt_f and ρ_f values of $595.24 \mu s m^{-1}$ and $1000 kg m^{-3}$. The effective porosity, φ_{eff} , at each horizon was calculated as the average of the available porosity estimates by the three methods subject to the conditions above. Figs. 10 to 14 give depth versus φ_{den} , φ_{son} , φ_{d-n} and φ_{eff} plots for the Chad, the Kerri Kerri, the Fika, the Gongila and Bima Formations, and Fig. 15 is a similar plot for the whole well.

For the Chad Formation (Fig. 10), only estimates of φ_{son} were obtained, these therefore also constitute the estimates of φ_{eff} . The trend of φ_{son} estimates, in agreement with the lithology structure obtained from the trend of shaliness and described by a sixth degree polynomial having a goodness-of-fit of 0.4144, is interpreted to indicate a three-lithology formation, with the two more porous lithologies separated by a tighter one centered around the depth 250 m. Sixth degree polynomial trends having low to moderate fits best describe the variations with depth of the four porosity estimates for the Kerri Kerri Formation (Fig. 11). While the trend of φ_{son} appear to vary in the opposite direction to those of φ_{son} , φ_{d-n} and φ_{eff} , all four trends are interpreted to indicate a three-lithology formation, with the possibility of two others at the top and another at the base. Porosity estimates for the Fika Formation (Fig. 12) are best described by sixth degree polynomials having low to moderate fits, with the trends for φ_{son} and φ_{den} varying in opposite directions. All four trends are however interpreted to indicate a two-lithology formation, with the first lithology extending only for the first 200 m and the second extending for the rest of the depth. Two intrusions are also predicted towards the base of the formation.

Fig 13 gives the plots of the best polynomial trends for the variations of porosity estimates with depth for the Gongila Formation. While the trends for φ_{son} ,

φ_{den} and φ_{eff} are best described by sixth degree polynomials having very low fits, the trend for φ_{d-n} is described by an exponential function having an improved but still low fit. The trend of φ_{d-n} is interpreted to be insensitive to variations with depth while the trend of φ_{son} is interpreted to indicate only a single lithology, with the possibility of two others at the top and the base. The trends of both φ_{son} and φ_{eff} are interpreted to indicate a two-lithology formation also with the possibility of two others at the top and the base, in agreement with the lithology structure revealed by the trend of shaliness. Fig. 14 gives the plots of the best polynomial trends for the variation of porosity estimates with depth for the Bima Formation. The trend for φ_{d-n} , as those of the other trends, is described by a sixth degree polynomial having low fit. Its invariability with depth, as in the Gongila Formation, is considered insensitive to reveal the lithology structure of the formation. The other trends are interpreted to indicate only a three-lithology formation as opposed to five-lithology structure revealed from the shaliness trend.

At the level of the whole well, variations of porosity with depth (Fig. 15) are best represented by sixth degree polynomial trends having low to moderate goodness-of-fits. Bottom upwards, all the trends show the raising and waning of porosities, with the peaks and troughs occurring at different depth intervals for the four porosity estimates. For φ_{den} and φ_{d-n} , the trends are quite close and similar, reaching the first peak early at the middle of the Gongila Formation, the second at the interface between the Fika and Kerri Kerri Formations and the possibility of a third at depth of the Chad Formation. The troughs occur at the middle of the Fika and Kerri Kerri Formations. A single peak for the φ_{son} trend occurred at the middle of the Fika Formation, with the possibility of a second at the depth of the Chad Formation, while the trough occurred at the top of the Kerri Kerri Formation. The trend for φ_{eff} reached the first peak a little later in comparison to those of φ_{den} and φ_{d-n} , at the interface of the Gongila and Fika Formations, with the possibility of a second peak at the depth of the Chad formation, while its trough occurred towards the

base of the Chad Formation. In general, porosity appears to be roughly raising and waning with marine invasion, a pattern similar to the trend of shaliness.

Estimates of the sonic porosity, φ_{son} , for the Chad, the Kerri Kerri, the Fika, the Gongila and the Bima Formations average 0.206 ± 0.012 , 0.225 ± 0.009 , 0.488 ± 0.015 , 0.513 ± 0.017 and 0.295 ± 0.013 respectively (Table 3). Bottom upwards, the values appear to rise and wane in a pattern consistent with growth and decay of marine invasion. While not having estimates for the top-most Chad Formation, estimates of both φ_{RB} and φ_{d-n} average 0.219 ± 0.008 , 0.124 ± 0.007 , 0.106 ± 0.005 and 0.068 ± 0.003 , and 0.203 ± 0.004 , 0.164 ± 0.004 , 0.130 ± 0.003 and 0.073 ± 0.002 respectively for the four other formations. The two estimates give similar patterns for the variation of average porosities, decreasing downwards, in agreement with decompaction expectation. Estimates of φ_{eff} for the five named formations average 0.206 ± 0.012 , 0.219 ± 0.004 , 0.255 ± 0.006 , 0.244 ± 0.007 and 0.145 ± 0.005 respectively, in agreement with Samaila (2007), while the pattern is consistent with the growth and wane of average shaliness, and therefore related to the transgression and regression of marine environment in the area also.

To determine the porosity at deposition, the graphs of *depth* versus φ , *depth* versus $\ln \varphi$, *depth* versus $1/\varphi$ and $\ln(\text{depth})$ versus $\ln(1 - \varphi)$ for all four sets of porosity estimates were plotted. Values of the porosities of the formations at deposition, φ_o , were estimated using the equations of best fitting linear regression lines of various functions of the porosity estimates with depth. Values of φ_o for the Chad and Kerri Kerri Formations were calculated from the plots of $\ln(\text{depth})$ versus $\ln(1 - \varphi_{eff})$ to be 0.694 and 0.522 respectively. For the Fika Formation, φ_o was calculated to be 0.411 from the plot of *depth* versus φ_{d-n} . The Gongila is estimated to have φ_o value of 0.775 from the plot of *depth* versus φ_{eff} , while a value of 0.558 is obtained for the Bima Formation from the plot of *depth* versus φ_{son} . Table 3 also lists the φ_o values.

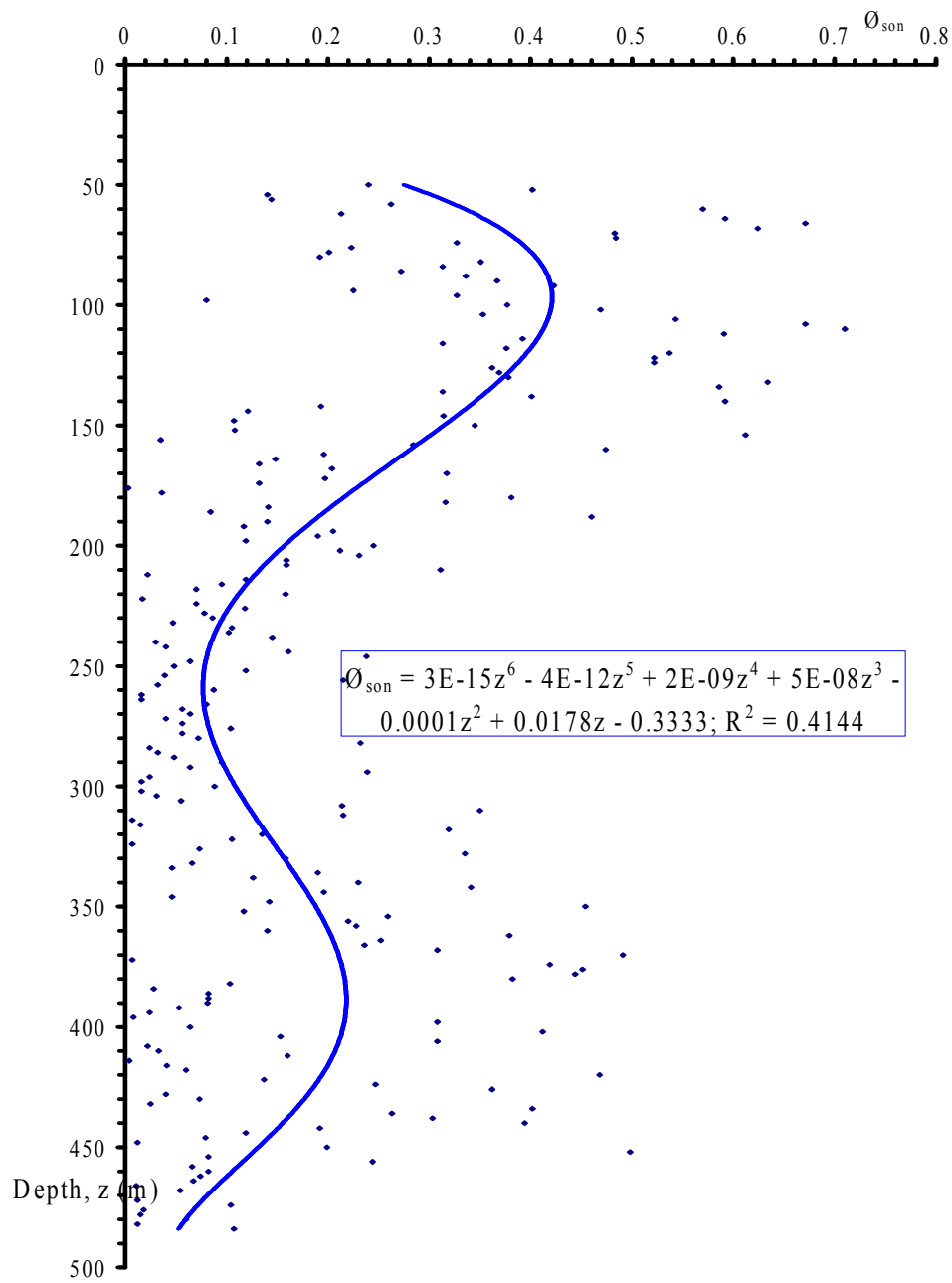


Fig. 10. Plot of depth versus best porosity estimates trend for the Chad Formation

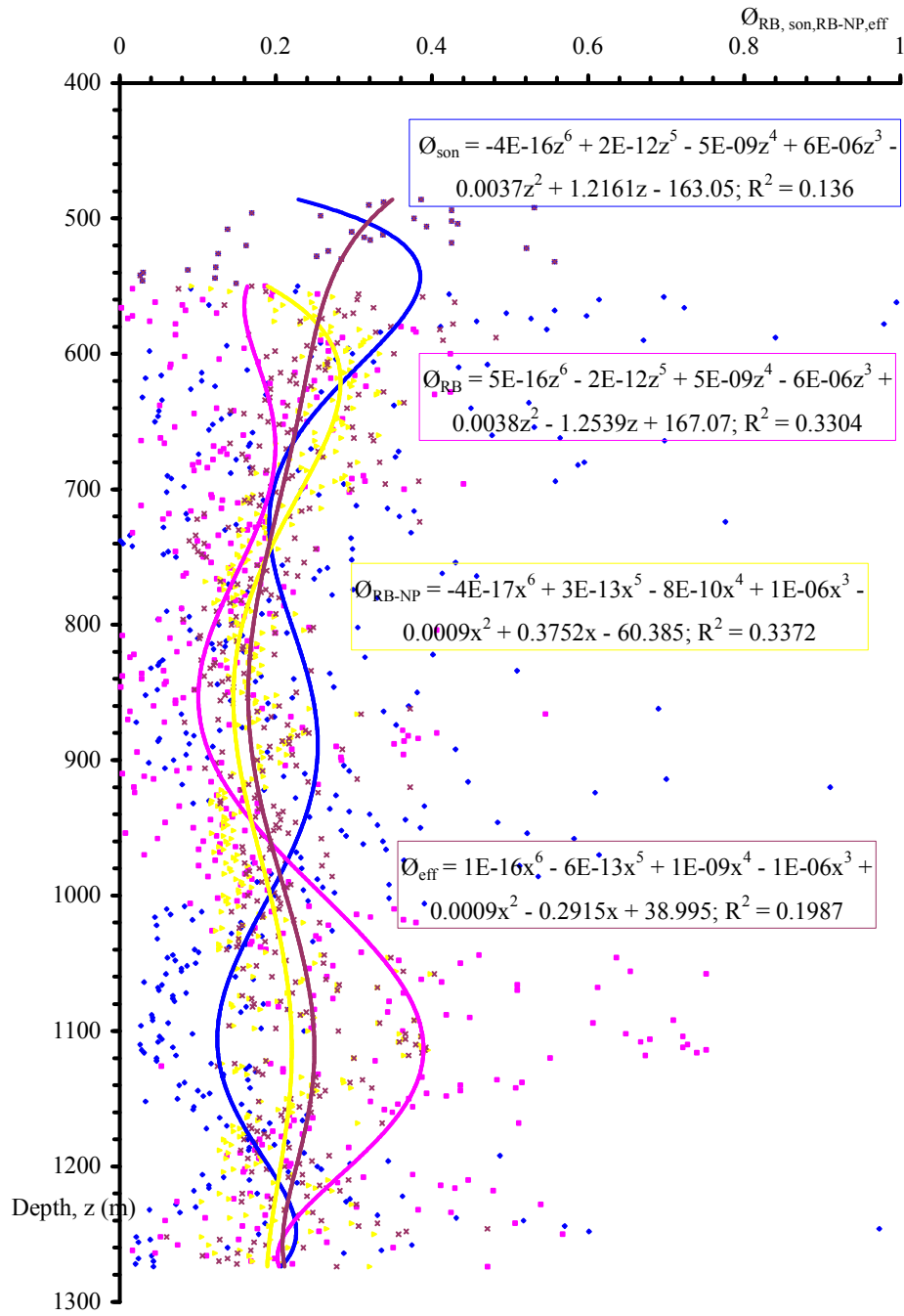


Fig. 11. Plots of depth versus best porosity estimates trends for the Kerri Kerri Formation

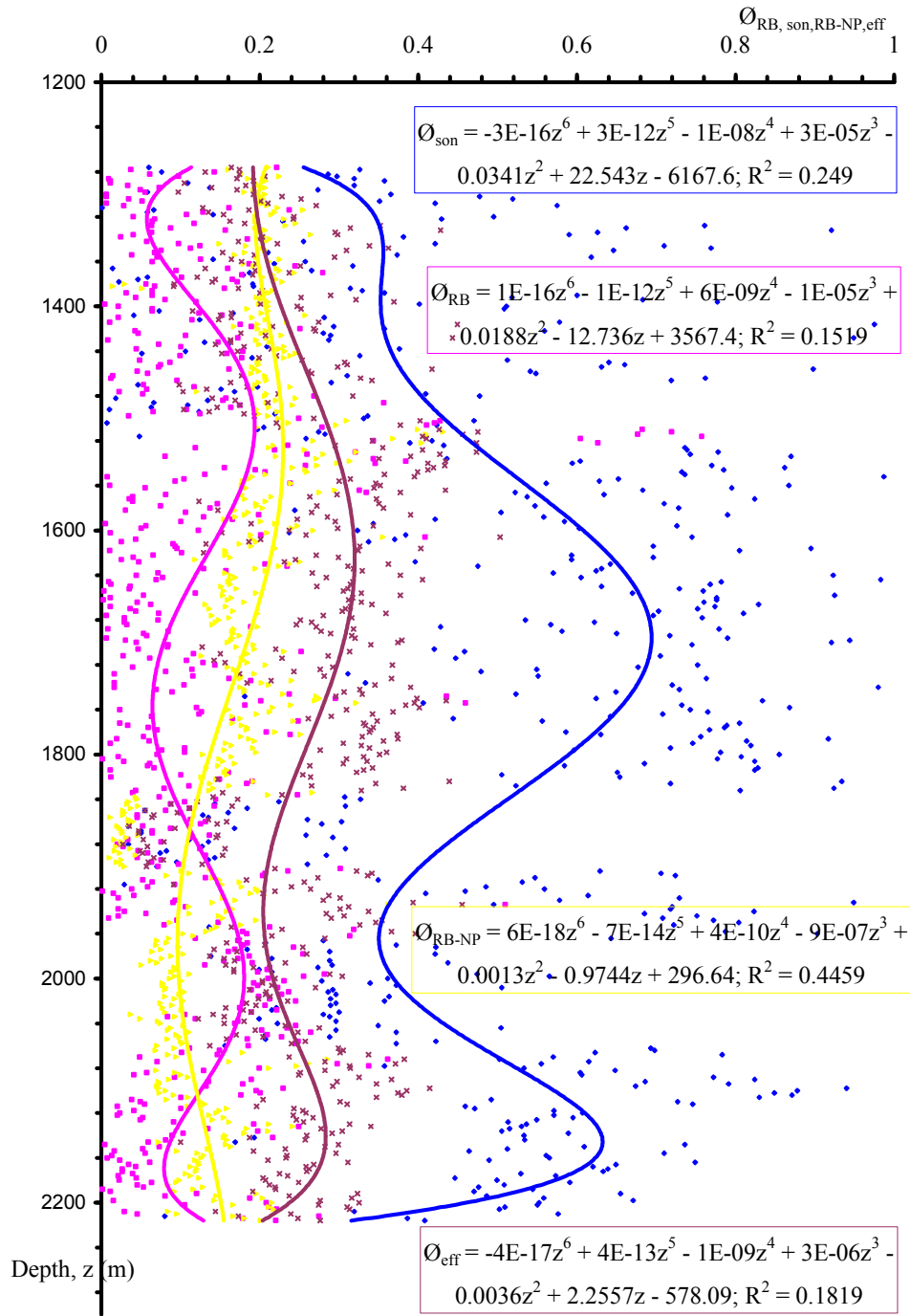


Fig. 12. Plots of depth versus best porosity estimates trends for the Fika Formation

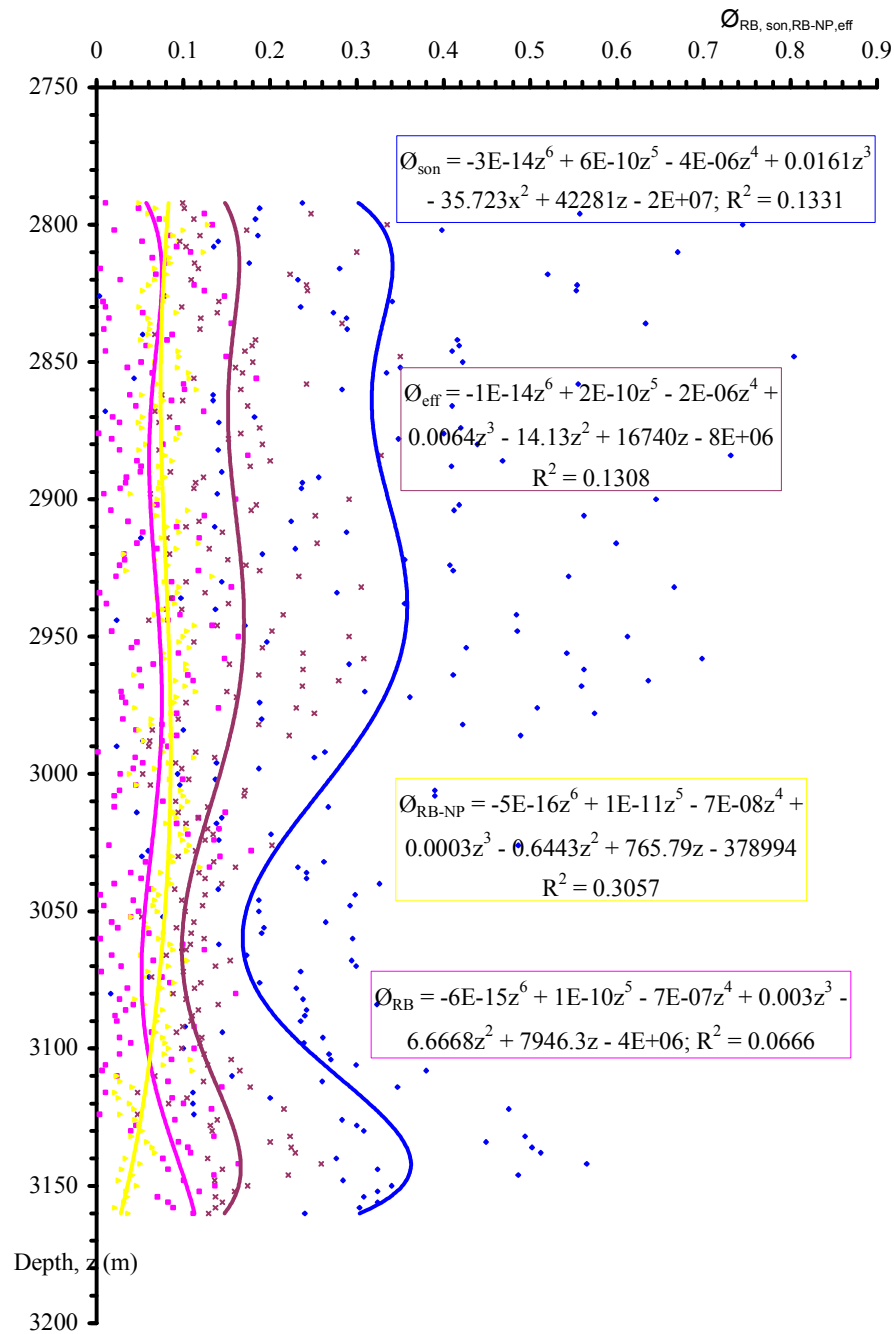


Fig. 13. Plots of depth versus best porosity estimates trends plots for the Gongila Formation

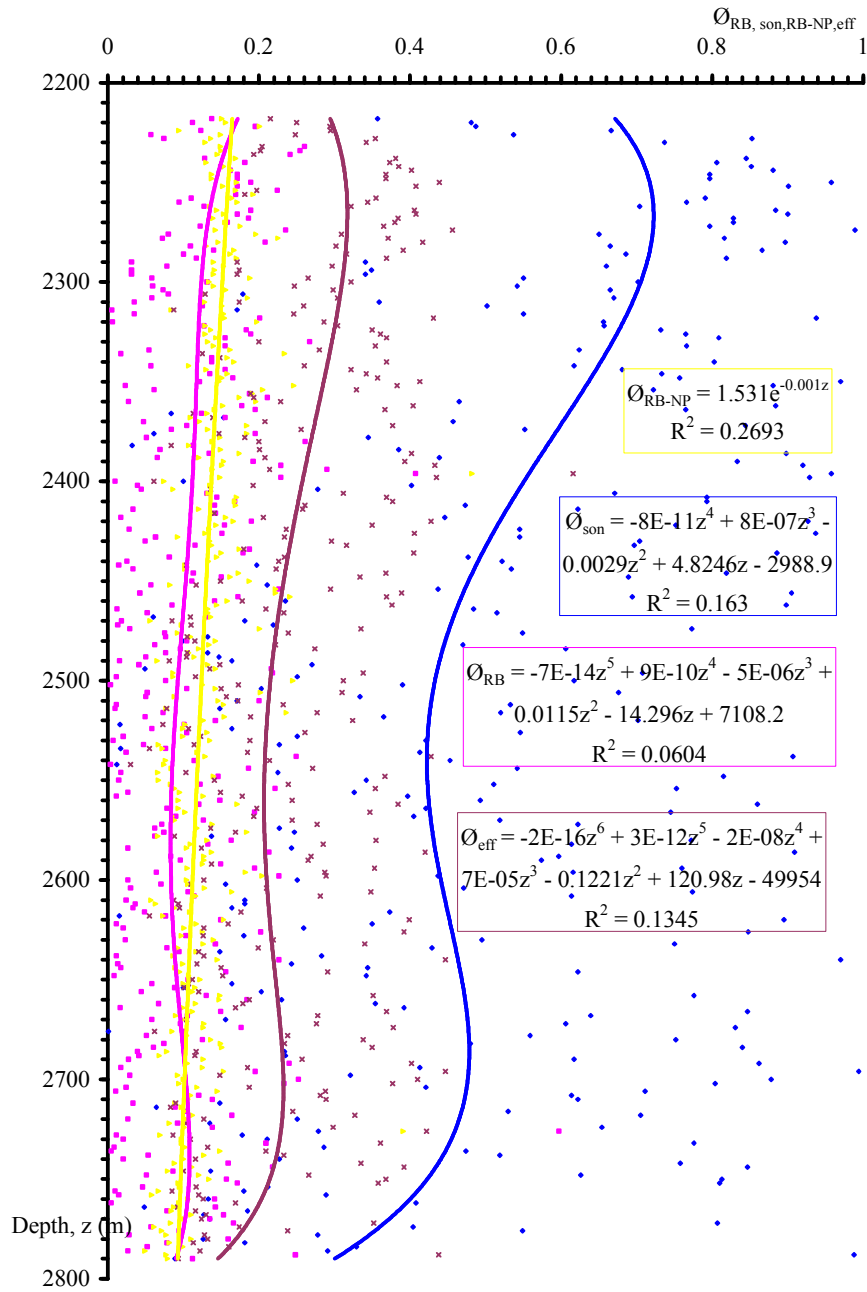


Fig. 14. Plots of depth versus best porosity estimates trends plots for the Bima Formation

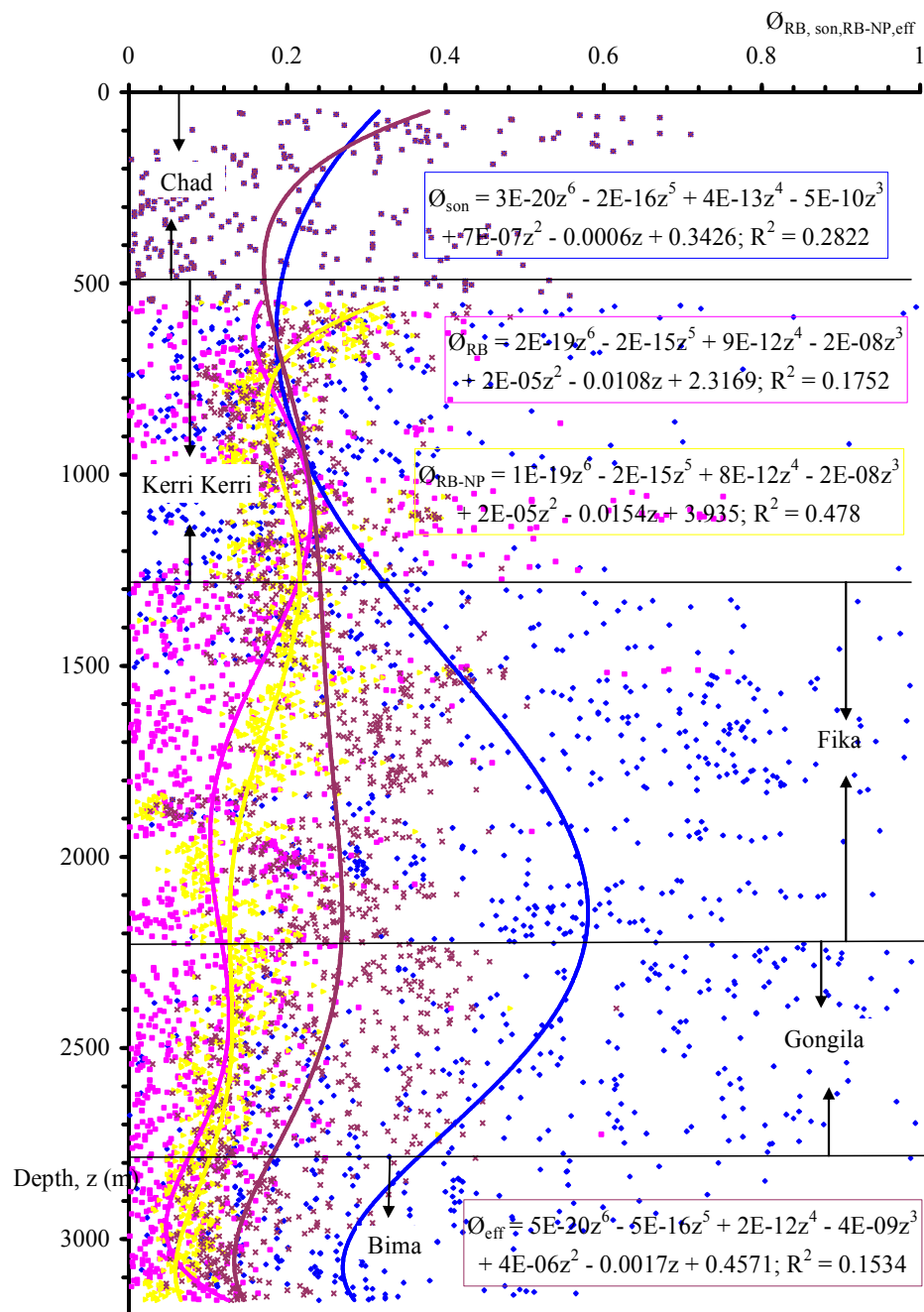


Fig. 15. Plots of depth versus best porosity estimates trends for the drilled column in the Faltu-1 well

Table 2. Goodness-of-fit for trend lines describing the variations of shaliness with depth.

Formation	V_{GR}	V_{SP}	V_{d-n}	V_{TH}	V_{eff}
Chad	0.606	0.680	-	-	0.592
Kerri Kerri	0.565	0.503	0.501	-	0.576
Gombe	-	-	-	-	-
Fika	0.272	0.271	0.581	0.170	0.305
Gongila	0.234	0.236	0.378	0.257	0.327
Bima	0.192	0.696	0.386	0.078	0.162
Column	0.311	0.656	0.609	0.296	0.196

Table 3. Average porosities of formations in the Faltu-1 well. φ_{den} is the bulk density porosity, φ_{sonic} is the sonic porosity, φ_{d-n} is the combined bulk density and neutron porosity, and φ_{eff} is the effective porosity. φ_o is the porosity at deposition.

Formation	φ_{son}	φ_{den}	φ_{d-n}	φ_{eff}	φ_o
Chad	0.206 ± 0.012	-	-	0.206 ± 0.012	0.694
Kerri Kerri	0.224 ± 0.009	0.219 ± 0.008	0.203 ± 0.003	0.219 ± 0.004	0.522
Gombe	-	-	-	-	-
Fika	0.488 ± 0.015	0.124 ± 0.007	0.164 ± 0.004	0.255 ± 0.006	0.411
Gongila	0.513 ± 0.017	0.106 ± 0.005	0.130 ± 0.003	0.244 ± 0.007	0.775
Bima	0.295 ± 0.013	0.068 ± 0.003	0.073 ± 0.002	0.145 ± 0.005	0.558
Column	0.361 ± 0.007	0.139 ± 0.003	0.154 ± 0.002	0.224 ± 0.003	0.329

COMPUTATIONS OF THERMAL CONDUCTIVITY

Three methods were employed for the estimation of thermal conductivities of drilled sedimentary rocks from the Faltu-1 well logs. The first is the method of Houbolt and Wells (1980). This empirical method estimates the thermal conductivity, λ_{HW} , of siliciclastic rocks with water-filled pores using only compressional sonic log. The method of Williams and Anderson (1990) was employed to calculate the second set of thermal conductivity estimates, λ_{WA} , using compressional and transverse sonic logs as well as the *RB* and *PEF* logs. The *PEF* log is only available from the depth of 1360 m to total depth, while the transverse sonic log is completely unavailable. The conversion of compressional sonic log to transverse wave velocities (Beardmore and Cull, 2001) allowed the use of the method to estimate λ_{WA} for the horizons where the *PEF* log is available. The Asquith (1991) method was employed for the estimation of the last set of thermal conductivity, λ_{ASQ} . The method requires the knowledge of both the effective shaliness and effective porosity of the drilled horizons. It also requires the input of the thermal conductivity of water (the assumed pore fluid), as well as those of the clay (shale) and matrix (sand) components. Shale and sand components were assigned thermal conductivities of 2.9 and 7.1 W m⁻¹ K⁻¹ respectively (Raznjevic, 1976; Majorowicz and Jessop, 1981; Roy et al., 1981; Reiter and Tovar, 1982; Reiter and Jessop, 1985; Drury, 1986; Taylor et al., 1986; Beach et al., 1987; Barker, 1996; and Beardmore, 1996). The thermal conductivity of water was calculated using the method of Touloukian et al. (1970). The three sets of thermal conductivity estimates were corrected for the effect of temperature using the method of Sekiguchi (1984). The effective thermal conductivity, λ_{eff} , was calculated as the mean of λ_{HW} , λ_{WA} and λ_{ASQ} .

Figs. 16 to 20 are depth versus λ_{HW} , λ_{ASQ} , λ_{WA} and λ_{eff} plots for the Chad, the Kerri Kerri, the Fika, the Gongila and the Bima Formations respectively, while Fig. 21 is a similar plot for the whole well. Fig. 16 gives the depth versus λ_{HW} , λ_{ASQ} and λ_{eff} plots for the Chad Formation. The estimates are best described by sixth degree polynomial trends having low to moderate goodness-of-fits. The trends show patterns that decrease with depth for a certain distance, and begin to rise again to values higher than those at the top. These are interpreted to blurredly indicate a three-lithology formation, in agreement with the trends of shaliness and porosity. Fig. 17 is a similar plot for the Kerri Kerri Formation. The trend for λ_{HW} is best described by a power function having a fit of 0.120, while the trends for λ_{ASQ} and λ_{eff} are best described by sixth degree polynomials with moderate fits. The trends are interpreted to blurredly indicate a three-lithology formation similar to that revealed by the trends of shaliness and porosity. The plots of depth versus λ_{HW} , λ_{ASQ} , λ_{WA} and λ_{eff} for the Fika Formation (Fig. 18) are best described by sixth degree polynomial trends having moderate fits, and are interpreted to indicate a two-lithology formation, with the top lithology extending to the depth of about 1500 m, and the second, though interrupted by intrusions, extending for the rest of the depth. The trend of λ_{eff} , exhibits a break at the depth of about 1370 m. This is the depth above which estimates of λ_{WA} did not exist. The break therefore is interpreted to highlight the difference between λ_{eff} estimated with and without contributions from λ_{WA} . The depth versus λ_{HW} , λ_{ASQ} , λ_{WA} and λ_{eff} plots for the Gongila Formation (Fig. 19) are best described by sixth degree polynomial trends having moderate goodness-of-fits. In agreement with the lithology structures revealed by the trends of both shaliness and porosity, thermal conductivity trends

are also interpreted to indicate, albeit blurredly, a two-lithology formation, the first extending down to about 2500 m. Trends of thermal conductivity estimates for the Bima Formation (Fig. 20) are best described by sixth degree polynomials having fits that vary from low through moderate to good. Although largely invariant for most of the depth extent of the formation, the trends may at best be described to indicate a two-lithology formation, contrary to the three- and five-lithology structures inferred from the trends of porosity and shaliness respectively.

At the level of the whole well, sixth degree polynomial functions of the depth, having low to moderate goodness-of-fits describe the variations of λ_{HW} , λ_{ASQ} , λ_{WA} and λ_{eff} (Fig. 21). The trends show thermal conductivity gently increasing with depth. This is interpreted to reflect the effects of sediments compaction in which sediments become denser and hence thermally more conductive with increasing depth. The trends also show the two breaks at the depth ranges of 1840 to 1900 and 1960 to 2060 m. These are attributed to intrusions. The trend for λ_{eff} shows another break at the depth of about 1370 m. This break is seen as indicative of significant differences between estimates of λ_{eff} for the deeper formations that were estimated using λ_{HW} , λ_{WA} and λ_{ASQ} and those for the shallower formations that were estimated using only λ_{HW} and λ_{ASQ} , and therefore need for correction. Fig. 22 gives the cross plots of λ_{eff} versus λ_{HW} , λ_{WA} and λ_{ASQ} . The plot of λ_{HW} versus λ_{eff} for the deeper formations (pink curve), has significantly higher fit of 0.924 in comparison to 0.607 for the shallower formations (blue curve). The need for the correction is also exhibited by the cross plot of λ_{ASQ} versus λ_{eff} , where the shallower and deeper formations give significantly different fits of 0.7658 and 0.5785 respectively. Although the cross plot of λ_{WA} versus λ_{eff} (red curve) for the deeper formation gave the best fit of 0.9456, the correcting equation taken to be $\lambda_{eff} = 2.1313 + 0.6294\lambda_{HW} \text{ W m}^{-1} \text{ K}^{-1}$.

Table 4 gives the average thermal conductivities of the formations encountered in the Faltu-1. Estimates of the effective thermal conductivity average 3.403 ± 0.004 , 3.592 ± 0.011 , 3.042 ± 0.004 , 3.012 ± 0.003 and $3.212 \pm 0.006 \text{ W m}^{-1} \text{ K}^{-1}$ for the Chad, the Kerri Kerri, the Fika, the Gongila and the Bima Formations respectively. Excluding the Gombe Formation, trends of average thermal conductivity exhibit a similar pattern (Fig. 23) which, bottom upwards, shows average thermal conductivity decreases up to the Fika Formation. The pattern then rises for the Kerri Kerri Formation and thereafter drops for the Chad Formation. The growth and wane of average thermal conductivity appears to be related to marine transgression and regression, reversely similar to patterns of growth and waning of average effective shaliness and average effective porosity. The availability of sonic log against the Gombe Formation from five other wells in the basin along with the correcting equation allowed for the computation of both its average λ_{HW} and λ_{eff} . Average thermal conductivity estimates for the Gombe Formation appear out of pattern, and suggest the average thermal conductivity of the formations may not remain consistent laterally across the basin as assumed. Assuming, however, that the thermal conductivities of the formations remain invariant across the basin allowed for the computation of well site average thermal conductivity. Map view of the result (Fig. 24) reveals a general trend that increases northeastward, from values of about $3.14 \text{ W m}^{-1} \text{ K}^{-1}$ around the Gubio and Maiduguri sub-basins in the South to values of about $3.30 \text{ W m}^{-1} \text{ K}^{-1}$ north of Bulte-1 well. In the three survey areas, patterns of thermal conductivity variations appear to follow or at least be influenced by the trends of the structural Highs. In the northern survey area, trends of thermal conductivity variations align with the trend of the Arege - Marte High, while in the Gubio and Maiduguri survey areas, the patterns are aligned to the Gubio and Maiduguri Highs.

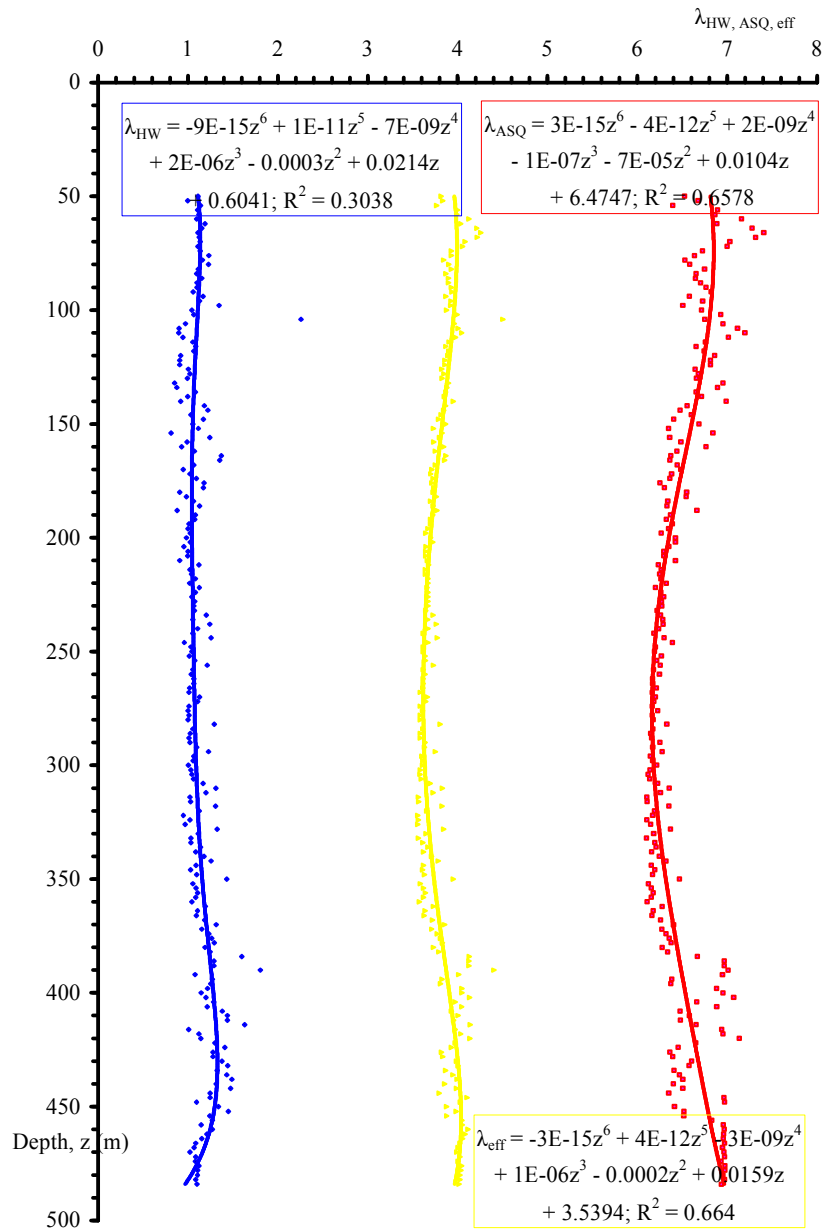


Fig. 16. Depth versus thermal conductivity ($W m^{-1} K^{-1}$) plots for the Chad Formation

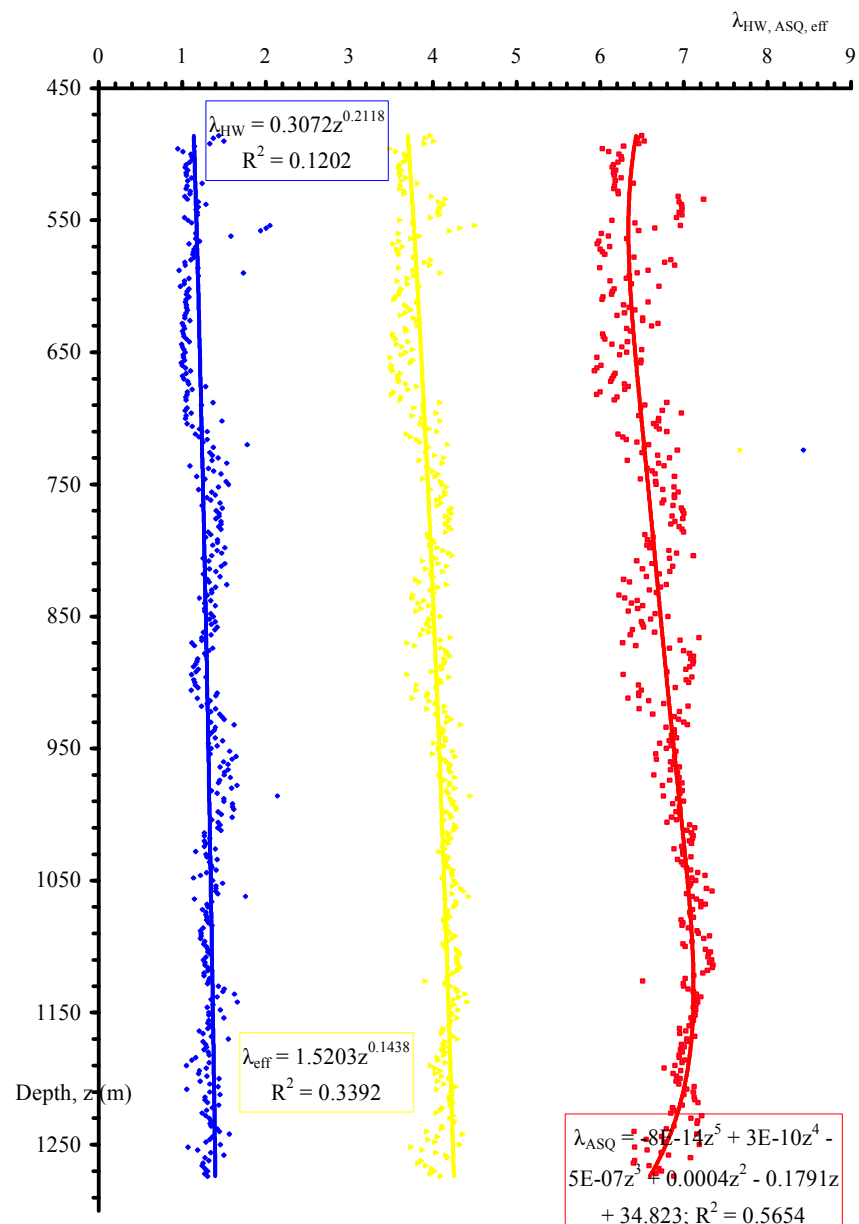


Fig. 17. Depth versus thermal conductivity ($\text{W m}^{-1} \text{K}^{-1}$) plots for the Kerri Kerri Formation

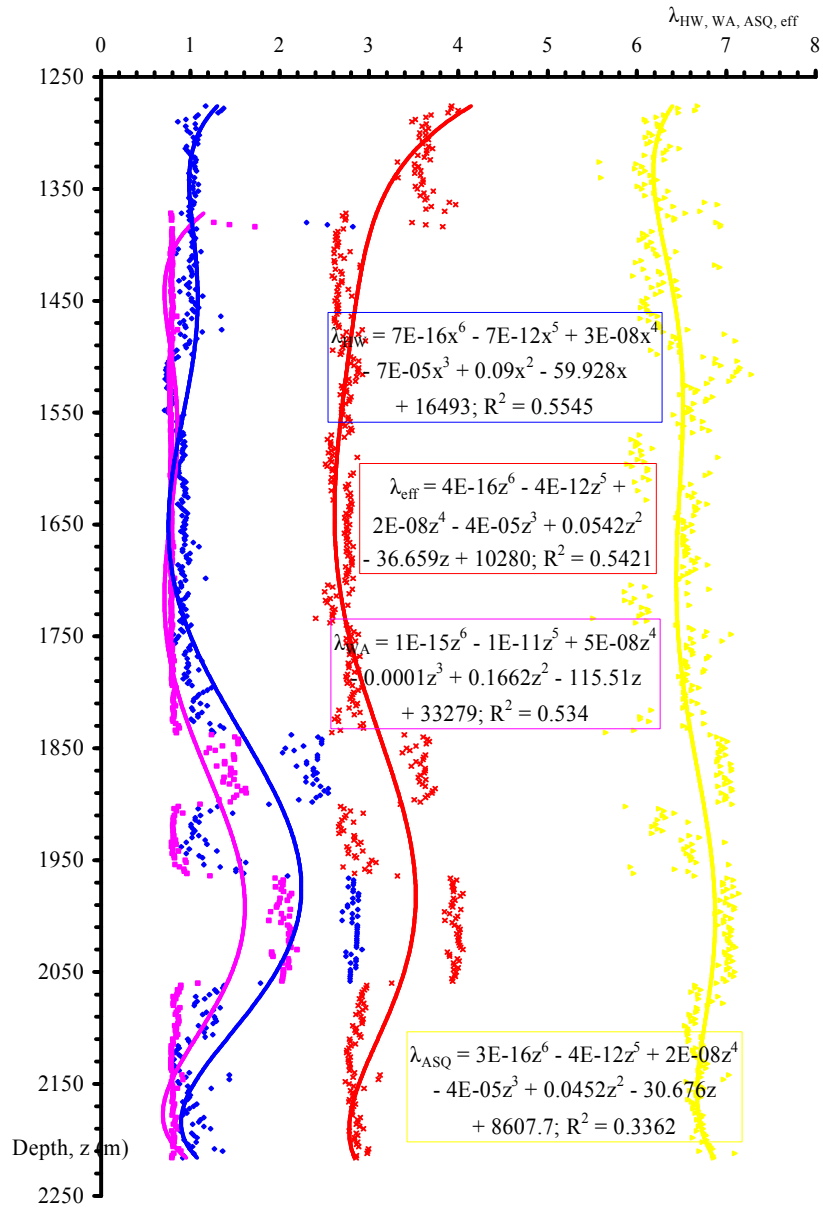


Fig. 18. Depth versus thermal conductivity ($W\ m^{-1}\ K^{-1}$) plots for the Fika Formation

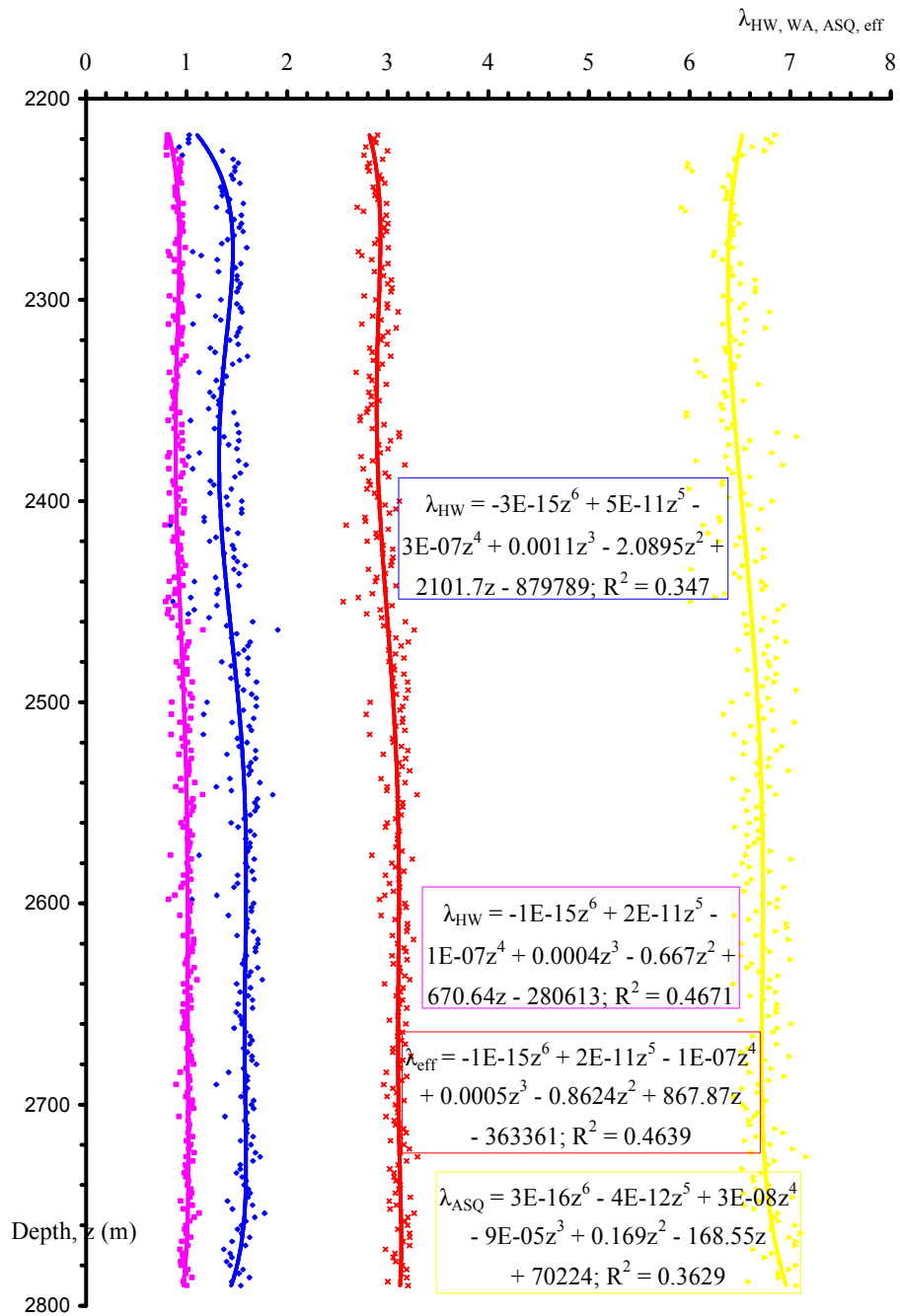


Fig. 19. Depth versus thermal conductivity plots ($W m^{-1} K^{-1}$) for the Gongila Formation

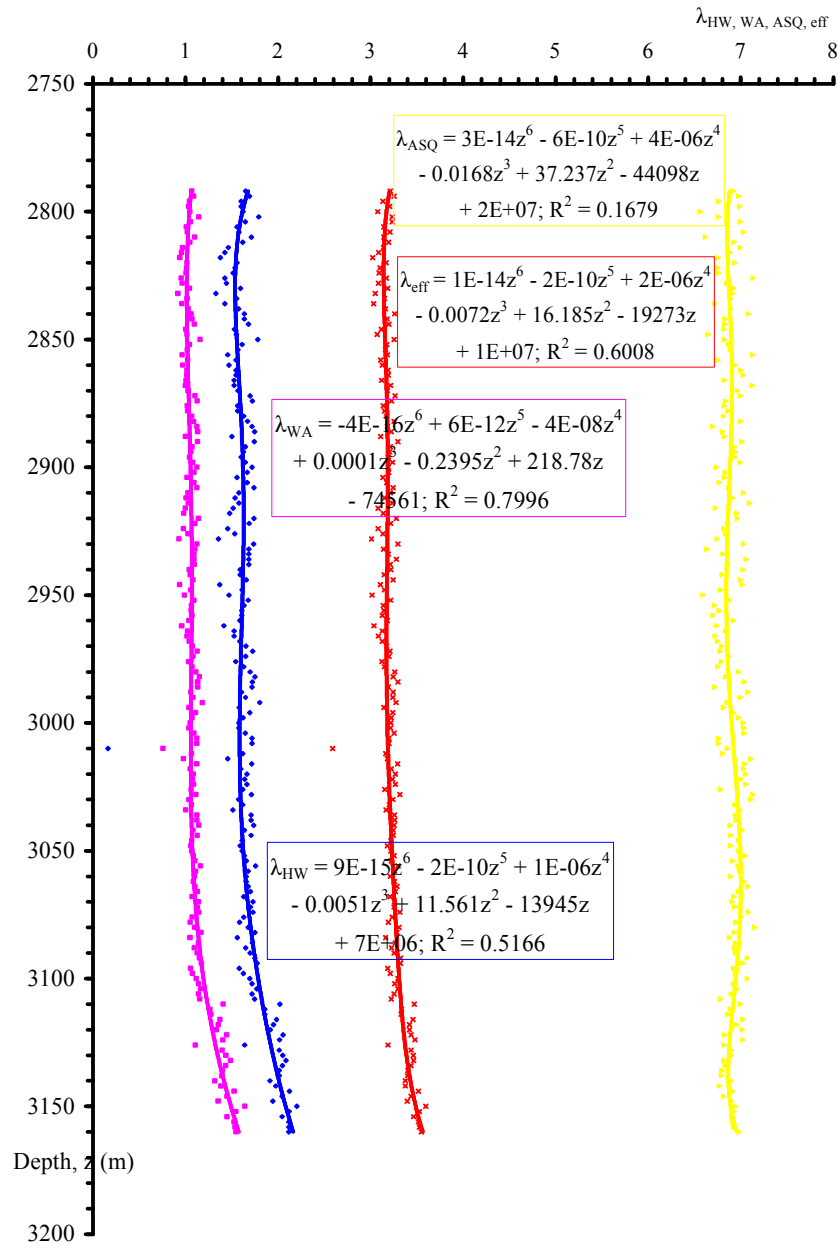


Fig. 20. Depth versus thermal conductivity ($W m^{-1} K^{-1}$) plots for the Bima Formation

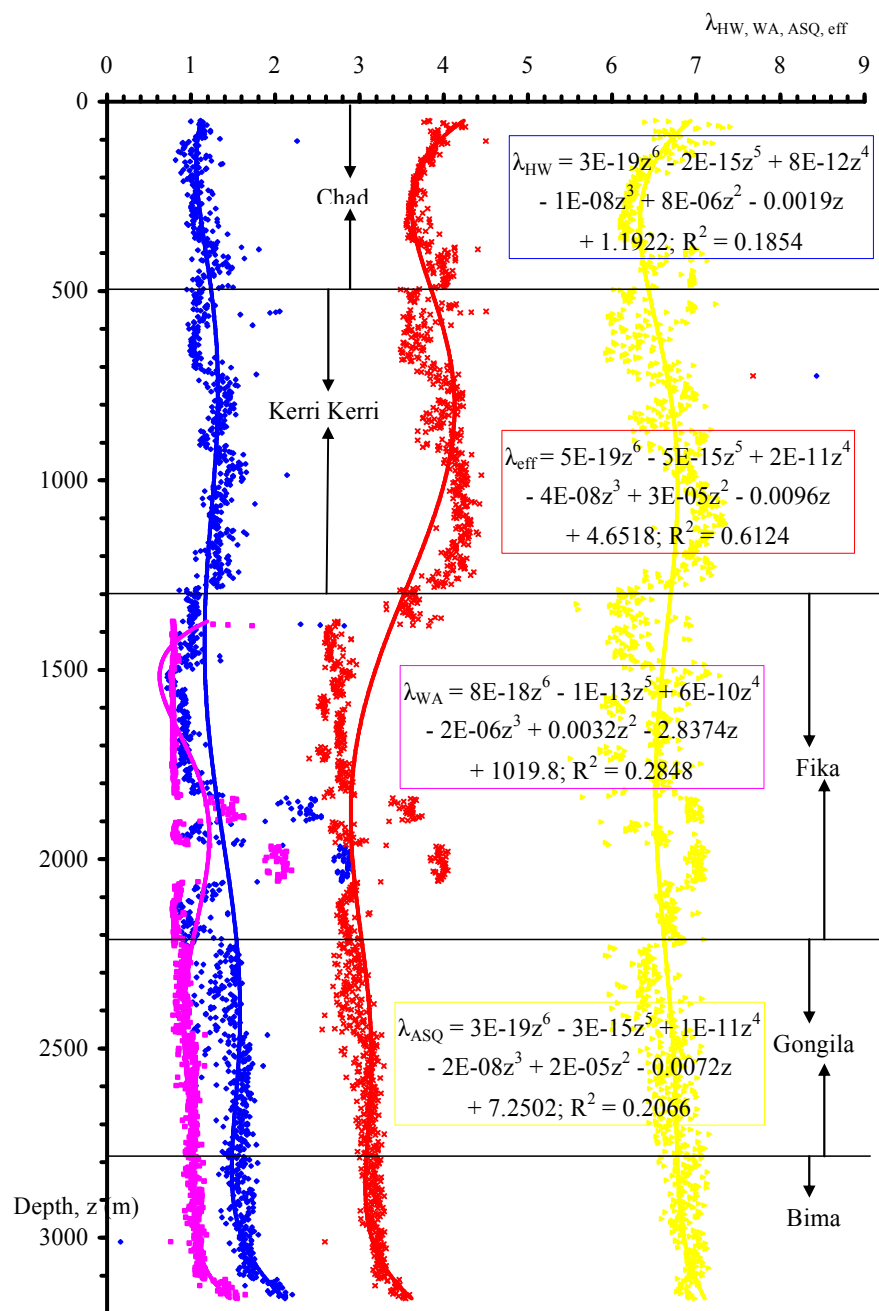


Fig. 21. Depth versus thermal conductivity ($\text{W m}^{-1} \text{K}^{-1}$) plots for the drilled column in the Faltu-1 well.

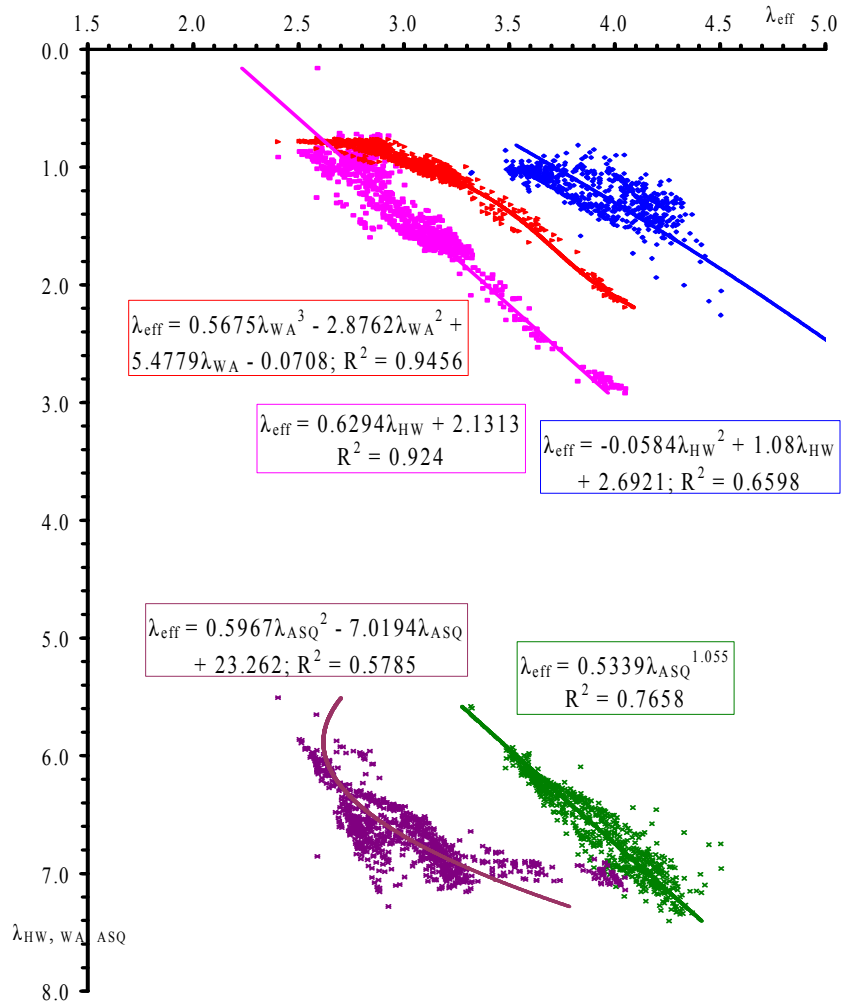


Fig. 22. Cross plots of best fitting trends λ_{eff} versus λ_{HW} (blue curve for shallow depths and pink curve for the deeper), λ_{WA} (red curve) and λ_{ASQ} (green curve for the shallow formations and violet curve for the deeper formations). Unit of thermal conductivity is $W m^{-1} K^{-1}$.

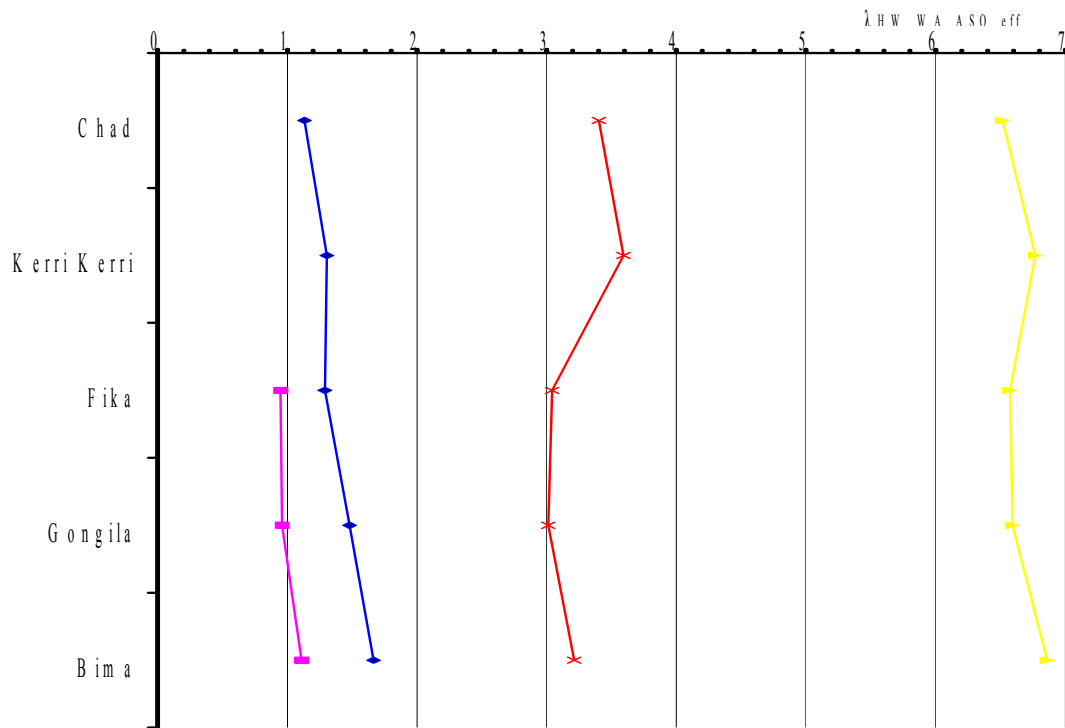


Fig. 23. Patterns of average thermal conductivity ($W m^{-1} K^{-1}$) trends for λ_{eff} (red), λ_{HW} (blue), λ_{WA} (pink) and λ_{ASQ} (yellow).

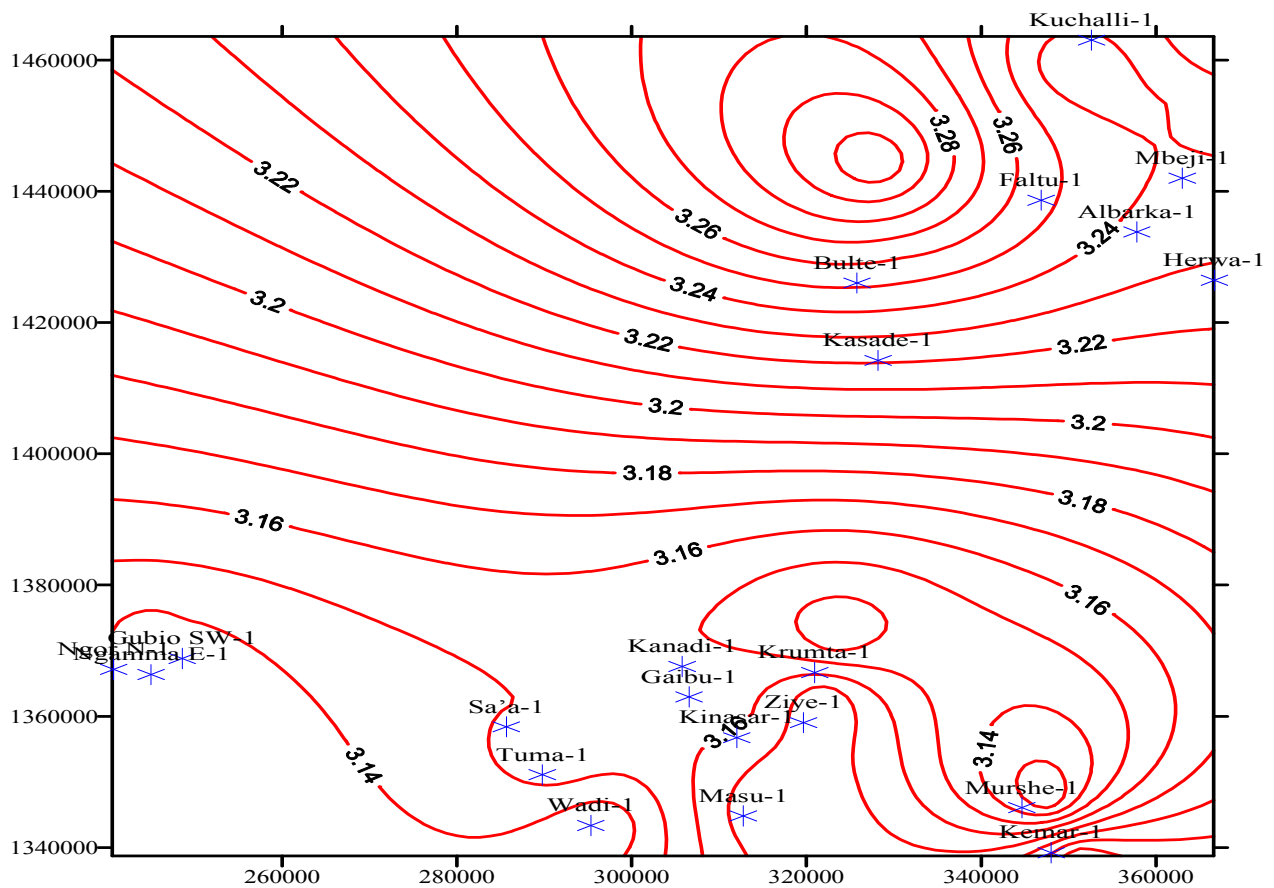


Fig. 24. Well site average thermal conductivity ($W m^{-1} K^{-1}$). Average thermal conductivity was assumed for wells (Gaibu-1, Herwa-1, Kuchalli-1) without required information to calculate their individual conductivities.

Table 4. Average thermal conductivity, λ ($\text{W m}^{-1} \text{K}^{-1}$) estimates of formations in the Faltu-1 well. Value marked ($\hat{\cdot}$) is the average for the formation from other wells for which the necessary data, sonic log, is available. Value marked (***) is estimated from correlation of average λ_{eff} with λ_{WA} . Values marked (+) are corrected for the absence of contribution from λ_{WA} , while value marked (***) is the average for the section having contributions from λ_{WA} .

Formation	λ_{HW}	λ_{WA}	λ_{ASQ}	λ_{eff}
Chad	1.132 ± 0.007	-	6.518 ± 0.006	$3.403 \pm 0.004^+$
Kerri Kerri	1.306 ± 0.019	-	6.769 ± 0.004	$3.592 \pm 0.011^+$
Gombe	$1.366 \pm 0.171^*$	-	-	$2.991 \pm 0.108^{***}$
Fika	1.289 ± 0.005	0.948 ± 0.005	6.572 ± 0.004	3.042 ± 0.004
Gongila	1.480 ± 0.004	0.960 ± 0.001	6.594 ± 0.004	3.012 ± 0.003
Bima	1.666 ± 0.011	1.109 ± 0.005	6.860 ± 0.003	3.212 ± 0.006
Column	1.351 ± 0.005	1.006 ± 0.034	6.653 ± 0.001	$3.038 \pm 0.011^{**}$

CONCLUSIONS

Three petrophysical properties: shaliness, porosity and thermal conductivity were estimated from well log data obtained from the Faltu-1 well, drilled in the Chad Basin, NE Nigeria. Shaliness was estimated using four independent methods, and polynomial trends of high degree and low to moderate fits best describe the variation of shaliness with depth. The trends were interpreted to delineate the possible number of lithologies in the formations as well as to link shaliness variation to the geologic history of the basin. Assessment of the contributions of the methods to the effective shaliness, obtained as the minimum of the four estimates, revealed that the thorium- and gamma ray-based methods significantly contribute more compared to the methods based on the combine bulk density and neutron porosity and self potential. The shaliness estimates derived from the gamma ray log, V_{GR} , vary between 0.019 and 0.990, average 0.161 ± 0.002 in the whole well, and 0.243 ± 0.008 , 0.106 ± 0.004 , 0.157 ± 0.003 , 0.211 ± 0.005 and 0.111 ± 0.003 in the Chad, the Kerri Kerri, the Fika, the Gongila and the Bima Formations respectively. SP-derived shaliness, V_{SP} , range between 0.006 and 0.561, average 0.266 ± 0.003 in the well and 0.170 ± 0.003 , 0.290 ± 0.002 , 0.373 ± 0.003 , 0.210 ± 0.002 and 0.143 ± 0.006 in the named formations respectively, while thorium-derived shaliness, V_{TH} , vary between 0.028 and 0.967, average of 0.426 ± 0.006 in the well, and 0.261 ± 0.009 , 0.170 ± 0.007 and 0.071 ± 0.003 in the Fika, Gongila and Bima Formations. The shaliness estimates derived from the combined bulk density and neutron porosity, $V_{\text{d-n}}$, range between 0.007 and 0.996, average of 0.193 ± 0.005 in the well, and 0.502 ± 0.006 , 0.562 ± 0.010 , 0.257 ± 0.007 and 0.192 ± 0.007 in the five named formations, while the effective shaliness, V_{eff} , vary between 0.006 and 0.351, average 0.121 ± 0.002 in the well, and 0.100 ± 0.001 , 0.138 ± 0.001 , 0.145 ± 0.003 , 0.135 ± 0.001 and 0.061 ± 0.009 in the formations.

Similarly also, porosity was estimated using three methods, and high-degree polynomial trends having low to moderate fits describe its variations with depth. The possible number of lithologies delineated from the trends largely agreed with those delineated from the trends of shaliness. Porosity estimated using the sonic log, φ_{son} , average 0.206 ± 0.012 , 0.224 ± 0.009 , 0.488 ± 0.015 , 0.513 ± 0.017 and 0.295 ± 0.013 for the Chad, Kerri Kerri, Fika, Gongila and Bima Formations respectively, while those estimated using the

bulk density log, φ_{den} , average 0.219 ± 0.008 , 0.124 ± 0.007 , 0.106 ± 0.005 and 0.068 ± 0.003 for the Kerri Kerri, Fika, Gongila and Bima Formations. The porosity estimates from the combined bulk density and neutron porosity logs, $\varphi_{\text{d-n}}$, 0.203 ± 0.003 , 0.164 ± 0.004 , 0.130 ± 0.003 and 0.073 ± 0.002 for the Kerri Kerri, Fika, Gongila and Bima Formations respectively. The five named formations were estimated to have average effective porosities of 0.206 ± 0.012 , 0.219 ± 0.004 , 0.255 ± 0.006 , 0.244 ± 0.007 and 0.145 ± 0.005 for the respectively, while their porosities at deposition, φ_0 , were estimated to be 0.694, 0.522, 0.411, 0.775 and 0.558.

Thermal Conductivities of drilled sedimentary formations were estimated using the methods Houbolt and Wells (1980), λ_{HW} , William and Anderson (1990), λ_{WA} , and the Asquith (1991), λ_{ASQ} . High-degree polynomial trends having low to moderate goodness-of-fits best describe depth versus thermal conductivity plots. Possible number of lithologies inferred from the trends agreed with those inferred from the trends of shaliness and porosities. Although conductivity estimates appear to wane and grow in patterns opposed to those of the shaliness, the trends are similarly interpreted to reflect the geologic history of the area. The trends also revealed significant differences between effective thermal conductivities of the shallower formations in comparison to those of the deeper ones, and therefore needed to be corrected. Linear regression lines fitted to the cross plots of the λ_{eff} versus λ_{HW} gave a fit of 0.924 for the deeper formation as compared to a fit of 0.607 for the shallower ones. Thermal conductivity estimates for the shallower formations were thus corrected using the relation $\lambda_{\text{eff}} = 2.1313 + 0.6294\lambda_{\text{HW}}$. Following the correction, the average effective thermal conductivities of the Chad and Kerri Kerri Formations were estimated to be 3.403 ± 0.004 and $3.592 \pm 0.011 \text{ W m}^{-1} \text{ K}^{-1}$, while those of the Fika, the Gongila and Bima Formations were estimated to be 3.042 ± 0.004 , 3.012 ± 0.003 and $3.212 \pm 0.006 \text{ W m}^{-1} \text{ K}^{-1}$. Estimates of λ_{HW} and λ_{ASQ} average 1.132 ± 0.007 , 1.306 ± 0.019 , 1.289 ± 0.005 , 1.480 ± 0.004 and $1.666 \pm 0.011 \text{ W m}^{-1} \text{ K}^{-1}$, and 6.518 ± 0.006 , 6.769 ± 0.004 , 6.572 ± 0.004 , 6.594 ± 0.004 and $6.860 \pm 0.003 \text{ W m}^{-1} \text{ K}^{-1}$ respectively for the named formations, while estimates of λ_{WA} average 0.948 ± 0.005 , 0.960 ± 0.001 and $1.109 \pm 0.005 \text{ W m}^{-1} \text{ K}^{-1}$ for the Fika, the Gongila and the Bima Formations. The availability of sonic log against the Gombe Formation from nearby wells allowed for the computation of its

average λ_{HW} and λ_{eff} as 1.366 ± 0.171 and 2.991 ± 0.108 while the assumption that thermal conductivities of formations laterally persisted across the basin also allowed for the computation of well site thermal conductivities. The map view of these well site conductivities revealed northeastward increase whose pattern align with the structural highs.

ACKNOWLEDGMENT

We wish to acknowledge the Nigerian National Petroleum Corporation, NNPC, for the main data used and for access to many confidential reports. We also thank colleagues, both at the in Physics and Geology Programmes of A.T.B. University for comments and criticism that have helped us improve the clarity of some of our arguments.

REFERENCES

- Allix, P.E., Grosdidier, E., Jardine, S., Legeox, O. and Popoff, M., 1981. Decouverte d'Aptien Superieur a Albuin inferieur date par microfossiles dans la serie detritique (Nigeria): Comptes Rendus de l'Academie des Sciences, Serie 11, 292, 1291 - 4.
- Asquith, G., 1991. Log Evaluation of Shaly Sandstones: A Practical Guide, AAPG Continuing Education Course Note Series (31): Tulsa, Oklahoma.
- Asquith G.B. and Gibson, C.R., 1982. Basic Well Log Analysis for Geologists, Tulsa, Oklahoma, AAPG.
- Avbovbo, A.A., Ayoola, E.O. and Osahon, G.A. 1986. Depositional and structural styles in Chad basin of northeastern Nigeria. AAPG Bull. 80: 1787 - 98.
- Barker, C., 1996. Thermal Modeling of Petroleum Generation: Theory and Applications. Elsevier, Amsterdam.
- Beach, R.D., Jones, F.W. and Majorowicz, J.A. 1987. Heat flow and heat generation estimates for the Churchill Basement of the Western Canadian Basin in Alberta, Canada. Geothermics. 16: 1 - 16.
- Beardsmore, G.R., 1996. The Thermal History of the Browse Basin and its Implications for Petroleum Exploration. Ph.D. dissertation, Monash University, Victoria, Australia.
- Beardsmore, G.R. and Cull, J.P. 2001. Crustal Heat Flow- A guide to measurement and modeling. Cambridge University Press, Cambridge.
- Beck, A.E., 1976. An improved method of computing the thermal conductivity of fluid-filled sedimentary rocks. Geophysics, 41: 133 - 44.
- Benkhelil, J. and Robineau, B., 1983. Le fosse de la Benoue est-il un rift? Bull. Centre Rech. Explor. Prod. Elf Aquitaine, 7(1): 315 - 21.
- Burke, K.C., 1976, The Chad basin, an active intra-continental basin, Tectonophysics, 36: 197 - 206.
- Carter, J.D., Barber W. and Tait, E.A. 1963. The geology of parts of Adamawa, Bauchi and Bornu Provinces in Northern Nigeria, Geological Survey of Nigeria. Bull. 30.
- Clauser, C. and Huenges, E. 1995. Thermal conductivity of rocks and minerals. In Rock Physics and Phase relation: A handbook of Physical constants . T.J. Ahrens (Ed.) AGU reference Shelf Series, AGU, Washington D.C. 3: 105 - 25.
- Cratchley, C.R., 1960. Geophysical survey of the Southern part of the Chad basin, Paper presented at CCTA conference on Geology, Kaduna, N. Nigeria.
- Dresser Atlas, 1982. Well logging and interpretation techniques, The course for home study, Dresser Atlas Publication.
- Drury, M.J., 1986. Thermal Conductivity, Thermal Diffusivity, Density and Porosity of Crystalline Rocks. Earth Physics Branch open file report (86-5): Ottawa: Earth Physics Branch.
- Genik, G.J., 1992. Regional framework, structural and petroleum aspects of rift basins in Niger, Chad and Central African Republic (C.A.R.). Tectonophysics. 213: 169 - 88.
- Genik, G.J., 1993. Petroleum geology of Cretaceous-Tertiary rift basins in Niger, Chad and Central African Republic. AAPG Bull. 77(8): 1405 - 34.
- GeoEngineering International, 1994. Re-appraisal of the hydrocarbon potential of the Nigerian sector of the Chad basin, NAPIMS, NNPC, Lagos, Nigeria. (confidential)
- Houbolt, J.J. and Wells, P.R.A., 1980. Estimation of heat flow in oil wells based on a relation between heat conductivity and sound velocity, Geol. Mijnbouw, 59: 215 - 24.
- Hunt, E. and Pursell, D., 1997. Fundamentals of log analysis, Part 7, Determining shaliness from logs, World Oil, 218(3): 55 - 8.
- Kappelmeyer, O. and Hanel, R., 1974. Geothermics with special reference to Application. Borntraeger, Berlin, Geoexplor. Monogr. Ser., 1(4): 238 pp.
- Majorowicz, J.A. and Jessop, A.M., 1981. Regional heat flow patterns in the Western Canadian sedimentary basin, Tectonophysics, 74: 209 - 38.
- Obi, G.C., 1996, The origin of the Bama- Maiduguri Ridge complex, northeastern Nigeria, deduced

- from pebble form indices, *Journal of Mining and Geology*, 32(1): 59 – 64.
- Onuoha, K.M. and Ekine, A.S., 1999. Subsurface temperature variations and heat flow in the Anambra basin, Nigeria, *Journal of African Earth Sciences*, 28(3): 641 - 52
- Raznjevic, K., 1976, *Handbook of Thermodynamic Tables and Charts*. Hemisphere Publishing Corporation, Washington DC.
- Reiter, M. and Jessop, A.M., 1985. Estimates of terrestrial flow in off-shore eastern Canada, *Canadian Journal of Earth Sciences*, 22: 1503 – 11.
- Reiter M.A. and Tovar, R.J.C., 1982. Estimates of terrestrial heat flow in Northern Chihuahua, Mexico, *Canadian Journal of Earth Sciences*, 22: 1512 – 7.
- Reyment, R.A., 1980. Biostratigraphy of the Saharan Cretaceous and Paleocene epicontinental transgression, *Cretaceous Research*, 1: 299 – 327.
- Rider, M.H., 1991. *The geological interpretation of well logs*, Whittles Publishing, Caithness.
- Robertson Group, 1989. The stratigraphy, sedimentology and geochemistry of the NNPC Tuma-1, Sa-1 and Kanadi-1 wells, drilled in the Nigerian Chad basin, Borno State, Nigeria. NNPC, Lagos, Nigeria. Report 4084/lb. (confidential)
- Robertson Group, 1991. The stratigraphy, sedimentology and geochemistry of the NNPC Ngamma East-1 and Gubio SW-1 wells, drilled in the Nigerian Chad Basin, Borno State, Nigeria, and correlation with the previously studied Tuma-1, Kanadi-1 and Sa-1 wells. NNPC, Lagos, Nigeria. Report 4531/lb. (confidential)
- Roy, R.F., Beck, A.E. and Touloukian, Y.S. 1981. Thermophysical properties of rocks. In *Physical Properties of Rocks and Minerals*. Y.S. Touloukian, W.R. Judd and R.F. Roy (Eds.), McGraw-Hill, New York. 409 – 502.
- Samaila, N. K., 2007. Reservoir potentials of the Upper Bima sandstone in the Yola and Lau-Lamurde basins, Upper Benue trough, NE Nigeria, Ph.D Thesis, A.T.B. University, Nigeria.
- Schlumberger, 1972. *Log interpretation manual/Principles*, vol. I, Schlumberger Well Services, Inc., Houston.
- Sekiguchi, K., 1984. A method for determining terrestrial heat flow in oil basinal areas. *Tectonophysics*, 103: 67 – 79.
- Serra, O., Baldwin, J. and Quirein, J., 1980. Theory, interpretation and practical application of natural gamma ray spectroscopy, Schlumberger, M.83214.
- Taylor A.E., Judge, A. and Allen, Y., 1986. Terrestrial heat flow from Project Cesar, Alpha Ridge, Arctic Ocean, *Journal of Geodynamics*, 6: 137 – 76.
- Touloukian Y.S., Liley, P.E. and Saxena, S.C., 1970. *Thermal Properties of Matter*, vol. 3, *Thermal Conductivity, Non-Metallic Liquids and Gases*. New York and Washington, IFI/Plenum.
- Vasseur G., Brigaud, F. and Demongodin, L., 1995. Thermal conductivity estimation in sedimentary basins, *Tectonophysics*, 244: 167 – 174.
- Williams C.F. and Anderson, R.N., 1990. Thermophysical properties of the earth's crust: In situ measurements from continental and ocean drilling, *Journal of Geophysical Research*, 95: 9209 – 36.
- Wylie, M.R.J., Gregory, A.R. and Gardner, G.H.F., 1958. An experimental investigation of the factors affecting elastic wave velocities in porous media, *Geophysics*, 23: 459 - 93.